NeuroImage: Clinical 17 (2018) 452–464

Contents lists available at ScienceDirect

NeuroImage: Clinical

journal homepage: www.elsevier.com/locate/ynicl

Local and distant relationships between amyloid, tau and neurodegeneration in Alzheimer's Disease

Leonardo Iaccarino[a,b,c,*,1], Gautam Tammewar[a,1], Nagehan Ayakta[a], Suzanne L. Baker[d,e], Alexandre Bejanin[a], Adam L. Boxer[a], Maria Luisa Gorno-Tempini[a], Mustafa Janabi[e], Joel H. Kramer[a], Andreas Lazaris[a,d], Samuel N. Lockhart[d], Bruce L. Miller[a], Zachary A. Miller[a], James P. O'Neil[e], Rik Ossenkoppele[a,d,f], Howard J. Rosen[a], Daniel R. Schonhaut[a,d], William J. Jagust[d,e], Gil D. Rabinovici[a,d,e]

[a] Memory and Aging Center, Sandler Neurosciences Center, University of California, San Francisco, CA 94158, United States
[b] Vita-Salute San Raffaele University, Milan 20132, Italy
[c] In Vivo Human Molecular and Structural Neuroimaging Unit, Division of Neuroscience, IRCCS San Raffaele Scientific Institute, Milan 20132, Italy
[d] Helen Wills Neuroscience Institute, University of California, Berkeley, CA 94720, United States
[e] Life Sciences Division, Lawrence Berkeley National Laboratory, Berkeley, CA 94720, United States
[f] Department of Neurology and Alzheimer Center, VU University Medical Center, Amsterdam 1081 HV, The Netherlands

ARTICLE INFO

Keywords:
Amyloid imaging
Tau imaging
Brain atrophy
Alzheimer's Disease
Dementia

ABSTRACT

The relationships between β-amyloid (Aβ), tau and neurodegeneration within Alzheimer's Disease pathogenesis are not fully understood. To explore these associations *in vivo*, we evaluated 30 Aβ PET-positive patients (mean ± sd age 62.4 ± 8.3) with mild probable AD and 12 Aβ PET-negative healthy controls (HC) (mean ± sd age 77.3 ± 6.9) as comparison. All participants underwent 3 T MRI, ^{11}C-PiB (Aβ) PET and ^{18}F-AV1451 (tau) PET. Multimodal correlation analyses were run at both voxel- and region-of-interest levels. ^{11}C-PiB retention in AD showed the most diffuse uptake pattern throughout association neocortex, whereas ^{18}F-AV1451 and gray matter volume reduction (GMR) showed a progressive predilection for posterior cortices ($p < 0.05$ Family-Wise Error-[FWE]-corrected). Voxel-level analysis identified negative correlations between ^{18}F-AV1451 and gray matter peaking in medial and infero-occipital regions ($p < 0.01$ False Discovery Rate-[FDR]-corrected). ^{18}F-AV1451 and ^{11}C-PiB were positively correlated in right parietal and medial/inferior occipital regions ($p < 0.001$ uncorrected). ^{11}C-PiB did not correlate with GMR at the voxel-level. Regionally, ^{18}F-AV1451 was largely associated with local/adjacent GMR whereas frontal ^{11}C-PiB correlated with GMR in posterior regions. These findings suggest that, in mild AD, tau aggregation drives local neurodegeneration, whereas the relationships between Aβ and neurodegeneration are not region specific and may be mediated by the interaction between Aβ and tau.

1. Introduction

Amyloid-β (Aβ) plaques, together with tau neurofibrillary tangles (NFT), are the neuropathological hallmarks of Alzheimer's Disease (AD) (Querfurth and Laferla, 2010). Aβ accumulation has been considered the initiating toxic event in AD, as posited by the *amyloid cascade hypothesis* (Hardy and Higgins, 1992). However, the relationships between amyloid accumulation, neurodegeneration and clinical decline are not straightforward (Chételat, 2013; Giacobini and Gold, 2013; Jack and Holtzman, 2013; Herrup, 2015). Significant levels of amyloid accumulation are found in approximately 30% of normal older individuals without evidence of clinically apparent cognitive decline (Jansen et al., 2015). Clinicopathological studies have revealed only modest correlations between Aβ accumulation, neurodegeneration and clinical state (Nelson et al., 2012; Murray et al., 2015; Jagust, 2016). Aβ reduction has thus far not yielded clear-cut significant clinical benefit in therapeutic trials in mild-to-moderate AD dementia (Doody et al., 2014; Salloway et al., 2014; Sevigny et al., 2016).

Conversely, the distribution and burden of NFTs shows a much tighter association with neurodegeneration and clinical status (Nelson

* Corresponding author at: Vita-Salute San Raffaele University, Nuclear Medicine Unit, IRCCS San Raffaele Hospital, Milan 20132, Italy.
E-mail address: iaccarino.leonardo@hsr.it (L. Iaccarino).
[1] These authors contributed equally.

http://dx.doi.org/10.1016/j.nicl.2017.09.016
Received 21 February 2017; Received in revised form 8 September 2017; Accepted 22 September 2017
Available online 25 September 2017

et al., 2012; Spires-Jones and Hyman, 2014; Murray et al., 2015). Recent advances in Positron Emission Tomography (PET) have led to the synthesis of radioligands with high affinity to the paired helical filament (PHF) tau aggregates seen in AD (Villemagne et al., 2015; Okamura et al., 2016). First reports on *in vivo* tau-PET imaging show significant relationships between tau ligand uptake and neurodegeneration across the continuum from pre-clinical AD to dementia (Ossenkoppele et al., 2015b; Brier et al., 2016; Chiotis et al., 2016; Johnson et al., 2016; Ossenkoppele et al., 2016; Schöll et al., 2016; Sepulcre et al., 2016; Cho et al., 2016a, 2016b; Bischof et al., 2016; Xia et al., 2017; Hanseeuw et al., 2017).

Neuropathology studies have shown that amyloid and tau accumulation follow distinct topographic patterns of early accumulation and progression across the AD continuum from preclinical disease to advanced dementia (Braak and Braak, 1991; Braak et al., 2006; Brettschneider et al., 2015), and these are used to stage AD neuropathological changes (Hyman et al., 2012; Montine et al., 2012). Amyloid aggregation begins in isocortical association areas and spreads *inwardly* to allocortex, limbic regions, and then brainstem and cerebellum. NFTs accumulate first in the entorhinal/transentorhinal cortex, before propagating into hippocampal regions and lateral temporal cortex followed by additional association cortices and finally primary unimodal cortices (Braak and Braak, 1991; Braak et al., 2006). While the interactions between Aβ and tau are incompletely understood, studies in both older healthy controls and symptomatic AD patients have found that tau extends to widespread neocortical areas primarily in subjects carrying a significant amyloid burden (Musiek and Holtzman, 2015; Johnson et al., 2016; Schöll et al., 2016; Lockhart et al., 2017; Pontecorvo et al., 2017; Hanseeuw et al., 2017; Vemuri et al., 2017).

This growing body of evidence depicts a synergistic but complex relationship between tau, β-amyloid and neurodegeneration. While there is considerable evidence supporting a promoting effect of amyloid accumulation on the spreading of neurofibrillary tau tangles outside the medial temporal lobe, the molecular basis of this influence remain elusive. *In vitro* and animal studies have shown that amyloid aggregates may promote seeding and spreading of tau aggregates (Bolmont et al., 2007; Vasconcelos et al., 2016; Duyckaerts et al., 2015; Musiek and Holtzman, 2015). Previous *in vivo* studies, however, have repeatedly shown that loci of significant amyloid accumulation do not necessarily bear significant tau pathology and *vice-versa* (Schöll et al., 2016; Cho et al., 2016a), highlighting the need for further research to uncover the molecular links between Aβ and tau. A better understanding of these relationships in the human brain could provide critical insight into disease mechanisms and help tailor therapeutic approaches. Multimodal neuroimaging investigations combining MRI and molecular imaging with PET allow for an *in vivo* exploration of these relationships at the whole-brain level. Previous studies investigating these relationships have focused on the pre-clinical or prodromal stages of AD (Sepulcre et al., 2016; Brier et al., 2016) rather than the fully symptomatic dementia stage, though biomarker associations are expected to be dynamic and evolve as the disease progresses (Jack et al., 2013). Here we applied voxel-based Biological Parametric Mapping (BPM) and Region-Of-Interest (ROI) analyses to assess local and distant relationships between Aβ, tau and neurodegeneration. Building on previous literature, we hypothesized that (i) presence of β-amyloid and tau would be related but show distinct spatial patterns, (ii) the topography of gray matter volume (GMV) reduction would more closely match tau accumulation than β-amyloid deposition, and (iii) β-amyloid ligand uptake would show the highest intra-modality correlations across cortical regions, whereas tau ligand binding and brain GMV reduction would show more restricted, regionally specific, intra-modality correlations.

2. Materials and methods

2.1. Participants

30 patients (mean age 62.4 ± 8.3 years, N = 18 females) with clinically probable AD dementia were included in the study. All were recruited from the University of California, San Francisco Memory and Aging Center (UCSF MAC). Consensus clinical diagnosis was established during a multidisciplinary conference attended by neurologists, neuropsychologists, and nurses after interviews with the patient and carepartner, neurological and neuropsychological evaluations. All patients met criteria for probable Alzheimer's Disease dementia established by the National Institute of Aging – Alzheimer's Association (McKhann et al., 2011). Nine patients met additional criteria for posterior cortical atrophy (PCA) (Mendez et al., 2002) and 7 for logopenic-variant of Primary Progressive Aphasia (lvPPA) (Gorno-Tempini et al., 2011), both recognized as atypical clinical variants of AD under current criteria (McKhann et al., 2011; Dubois et al., 2014). All patients were ^{11}C-PiB-positive based on both visual interpretations of elevated binding in neocortex and quantitative assessment (global ^{11}C-PiB Distribution Volume Ratio (DVR) > 1.20) (Villeneuve et al., 2015). All the multimodal correlation analyses in the present study were run on a pooled group including all patients. Biomarker patterns in individual AD variants have been previously described by our group and others (Ossenkoppele et al., 2016; Dronse et al., 2017).

A group of 12 healthy controls (HC, mean age 77.3 ± 6.8, N = 8 females) was recruited from the Berkeley Aging Cohort (Schöll et al., 2016). These participants also underwent 3T structural MRI, ^{11}C-PiB-PET and ^{18}F-AV1451-PET scans. All controls included in this study were amyloid-negative based on a quantitative ^{11}C-PiB-PET threshold validated *versus* post-mortem findings (global ^{11}C-PiB DVR < 1.08) (Villeneuve et al., 2015). The HC group was included in order to: (i) assess group-level differences in GMV and ^{11}C-PiB- and ^{18}F-AV1451-PET (AD patients *vs.* HC), and (ii) to generate both single-subject z-maps and regional z-scores used for multimodal correlations within the AD group (see below).

Informed consent was obtained from all subjects or their assigned surrogate decision-makers, and UCSF, University of California Berkeley, and the Lawrence Berkeley National Laboratory (LBNL) institutional review boards for human research approved the study.

2.2. Image acquisition

2.2.1. MRI

Patient MRIs were performed at the UCSF Neuroimaging Center and control MRIs were performed at UC Berkeley. All scans were obtained on 3-Tesla Siemens Tim Trio scanners using a T1-weighted volumetric magnetization prepared rapid gradient echo (MPRAGE) sequence (TR: 2300 ms, TE: 2.98 ms, TI: 900 ms, flip angle: 9°) and reconstructed as a 160 × 240 × 256 matrix with 1 mm^3 spatial resolution.

2.2.2. PET

PET scans were performed at Lawrence Berkeley National Laboratory on a Siemens Biograph 6 Truepoint PET/CT scanner in 3D acquisition mode with a low-dose CT/transmission scan preformed prior to each scan for attenuation correction. Both ^{11}C-PiB and ^{18}F-AV1451 were synthesized at Lawrence Berkeley National Laboratory Biomedical Isotope Facility as previously described (Schöll et al., 2016). For ^{11}C-PiB, a 90-minute scan was acquired immediately following intravenous injection of ~15 mCi of tracer. For ^{18}F–AV1451, ~10 mCi of tracer was injected intravenously and one of two acquisition parameters was followed: either 0–100 min (12 patients, 7 controls) or 75–115 min (18 patients, 5 controls). Scans were reconstructed as previously described (Ossenkoppele et al., 2016).

2.3. Image pre-processing

2.3.1. MRI pre-processing

MPRAGE sequences were segmented and regions of interest (ROIs) were defined in participant native space using Freesurfer 5.1 (Desikan et al., 2006). Freesurfer-derived cortical ROIs were combined to create metaROIs, while the cerebellar gray matter ROI was used to normalize PET scan intensity across subjects (see below).

2.3.2. PET pre-processing

PET images were coregistered to the patient's MPRAGE using Statistical Parametric Mapping (SPM) version 8 (Wellcome Trust Centre for Neuroimaging). Dynamic 90-minute ^{11}C-PiB scans were analyzed applying Logan graphical analysis (35–90 minute post-injection) with cerebellar gray matter (derived from Freesurfer segmentation) as the reference region (Logan et al., 1996). ^{18}F-AV1451 standard uptake value ratios (SUVRs) were created using the cerebellar gray matter reference region to normalize mean activity from 80 to 100 minute post-injection based on previous validation using kinetic modeling approaches (Baker et al., 2017).

When examining relationships between β-amyloid and tau, PET images were also corrected for partial volume effects using the 3-compartment partial volume correction (PVC) method (Müller-Gärtner et al., 1992) to adjust for potential contamination of gray matter regions with PET signal from white matter or CSF spaces. Gray matter, white matter and CSF probabilities used for PVC were derived from MRI segmentation in SPM. PET images were not PVC-corrected when testing the relationship between each tracer and brain GMV reduction due to the risk of artificially introducing dependency between the measurements and thus generating false positives.

2.4. Voxel-wise image creation

For voxel-wise analyses in template space, MPRAGE images were segmented into gray matter, white matter, and cerebrospinal fluid (CSF) probability masks using the Segment tool in SPM12. Diffeomorphic Anatomical Registration Through Exponentiated Lie algebra (DARTEL) was used to create a study-specific template (including both patients and HC) by aligning and normalizing the gray matter probability images to a common space (the DARTEL template) using individual flow fields for each image. Images were then spatially warped to Montreal Neurological Institute (MNI) space and smoothed by a 9.9 mm full width at half maximum (FWHM) isotropic Gaussian kernel to create final gray matter probability (GMP) maps matching the PET scans resolution. These GMP images were then divided by the total intracranial volume to obtain Gray Matter Volume (GMV) maps.

Both the PVC and the non-PVC PET images were spatially warped to MNI space (2 mm^3 resolution) using the individual flow fields created during MRI processing. These images were then smoothed by a 7.6 × 7.6 × 6.9 mm FWHM kernel to obtain a final resolution of 10 mm FWHM.

A gray matter mask was created by warping the gray matter segmentation for the DARTEL template to MNI space and binarizing the image to only include voxels that had at least a 30% gray matter probability. A further step was performed to exclude subcortical structures (basal ganglia, thalamus, cerebellum and brainstem) from the mask, to avoid inclusion of regions that show off-target ^{18}F-AV1451 binding likely unrelated to tau (Lowe et al., 2016). Finally, single-subject z-score maps were created for each modality (MRI, ^{11}C-PiB-PET and ^{18}F-AV1451-PET) using the mean and standard deviation from the HC scans.

Though HC were on average older than AD patients, only Aβ negative HC were included to minimize the potential impact of preclinical AD on the distribution of HC MRI and PET measures. The single-subject z-maps were used for all the subsequent multimodal analyses.

2.5. ROI extraction

ROI mean GM volumes, ^{11}C-PiB-DVR and ^{18}F-AV1451-SUVR values from both PVC and non-PVC images were extracted from Freesurfer-derived cortical ROIs (Desikan et al., 2006). Weighted average values from Desikan Atlas ROIs were used to define 13 metaROIs (see Supplementary file 1). These included: precuneus (by itself), anterior cingulate (caudal and rostral anterior cingulate), posterior cingulate (posterior cingulate and isthmus cingulate), superior parietal lobe (by itself), inferior parietal lobe (inferior parietal lobule, supramarginal gyrus), inferior frontal lobe (partes triangularis, opercularis, and orbitalis), middle frontal lobe (caudal and rostral middle frontal gyri), superior frontal lobe (superior frontal gyrus and frontal pole), orbitofrontal cortex (medial and lateral orbitofrontal cortex), medial temporal lobe (hippocampus, entorhinal cortex and parahippocampal gyrus), lateral temporal lobe (inferior, middle, and superior temporal gyri), medial occipital lobe (cuneus and lingual gyrus), and lateral occipital lobe (fusiform gyrus and lateral occipital cortex). Therefore, we considered a total of 26 metaROIs: 13 for each hemisphere when comparing patients and controls for each modality. For multimodal comparisons, we included nine additional areas to fully encompass all cortical regions delineated by the Desikan atlas, which additionally included the amygdala, banks of superior temporal sulcus, paracentral gyrus, pericalcarine cortex, postcentral gyrus, precentral gyrus, temporal pole, transverse temporal gyrus, and insula. These additional areas were included to best recapitulate the voxel-based analysis (see below) by covering all cortical and limbic regions, in contrast to the large metaROIs that were created to provide summary metrics for the individual biomarkers.

2.6. Gray matter volume reduction and protein accumulation at the voxel-level

The presence and extent of GMV reduction (GMR), Aβ (^{11}C-PiB-DVR) and NFT (^{18}F-AV1451-SUVR) accumulation was tested by means of separate two-sample *t*-test (all patients *vs*. HC) implemented in SPM12, entering age and sex as nuisance covariates. For PET tracers, significance was set at $p < 0.05$, Family-Wise Error (FWE) corrected, with a minimum cluster extent of $k = 100$ voxels. For GMR, the statistical threshold was set at $p < 0.0001$ (uncorrected for multiple comparisons), entering age and sex as nuisance variables. Multiple comparisons correction was not applied for MRI, considering the mild AD stage of the cohort, to allow adequate visualization of the GMR distribution while still setting a reasonably stringent statistical threshold. The FWE-corrected results are available in Supplementary file 2.

To evaluate at the voxel-level the local relationships between GMR, β-amyloid and tau accumulation within the patients group, we adopted a multivariate approach using Biological Parametric Mapping (BPM) (Casanova et al., 2007), a MATLAB toolbox integrated within SPM. The BPM approach employs the General Linear Model (GLM) and allows testing of voxel-level multiple regressions (or other designs) entering both imaging modalities and non-imaging variables in the analysis as either covariates or as variables of interest. In the present study, we entered the single-subject z-score maps of each modality for each patient into the BPM analysis adopting a multiple regression model and controlling for the presence of outliers (*bi-square* robust regression) (Yang et al., 2011). The explicit mask resulting from the DARTEL pipeline (see above) was used to constrain the analysis to cortical gray matter.

To evaluate the relationships between the three imaging modalities, we tested the following models:

1. GMV z-maps explained by ^{18}F-AV1451 SUVR z-maps, controlling for age, sex and ^{11}C-PiB DVR z-maps as imaging covariates. The same design was repeated substituting global cortical ^{11}C-PiB DVR

(calculated as the average of weighted mean values from Freesurfer-derived regions of interest in frontal, parietal, temporal, and posterior cingulate cortex) (Ossenkoppele et al., 2016) for the ^{11}C-PiB DVR images.
2. GMV z-maps explained by ^{11}C-PiB DVR z-maps, controlling for age, sex and ^{18}F-AV1451 SUVR z-maps as imaging covariates. Building on previous literature on regional specificity and variability of ^{18}F-AV1451 distribution across AD phenotypes (Ossenkoppele et al., 2016), we did not examine an alternative model substituting a global measure of cortical ^{18}F-AV1451 as was done for ^{11}C-PiB-GMV relationships.
3. ^{18}F-AV1451 PVC SUVR z-maps explained by ^{11}C-PiB PVC DVR z-maps, controlling for age and sex.

Significance for BPM was set at $p < 0.01$, False Discovery Rate (FDR) corrected with a minimum cluster extent of $k = 100$ voxels. Results were also displayed at more liberal thresholds, *i.e.* $p < 0.001$ and $p < 0.01$ uncorrected. These uncorrected thresholds were selected to assess underlying trends of correlation and for visualization purposes.

2.7. Gray matter volume reduction and protein accumulation at the ROI-level

GMR and protein accumulation were evaluated using Freesurfer-extracted metaROIs described above. ROI-based analyses were adopted to investigate long-distance regional relationships between modalities. This allows us to examine whether, for instance, protein aggregation in one region may promote neurodegeneration in a distant, but connected, second region. Indeed, the same approach was applied to amyloid-tau relationships, following evidence for possible long-distance dynamic interactions between the two proteinopathies (Sepulcre et al., 2016; Brier et al., 2016). The ROI approach also allows us to investigate local multimodal relationships in pre-defined anatomic regions in native space, providing corroborative evidence for the voxel-based associations found in template space with BPM. At the ROI-level, a complementary partial correlation approach was adopted to test the pairwise relationships between modalities. To maintain consistency between voxel- and ROI-level analyses, z-scores for each subregion were calculated and subsequently used for the partial correlation analyses which were run only within the AD patient group. Partial non-parametric Spearman coefficients were estimated among all the pairwise combinations of regional biomarkers. Age and sex were entered as confounding variables. For the model in which GMV z-scores were explained by ^{18}F-AV1451 SUVR z-scores, global ^{11}C-PiB DVR was included as covariate to mirror the voxel-based BPM approach. The resulting correlation matrices were then thresholded to keep only correlation coefficients significant at $p < 0.001$. For between-modality regional associations, both direction (within- or between-lobes) and correlation type (positive *vs*. negative) were considered. The number of significant inter-regional correlations and the average strength of the regional associations were estimated to evaluate intra-modality correlations across the three imaging measures.

2.8. Statistical analysis

Statistical analyses were implemented with RStudio software (R version 3.2.3 for MAC, https://www.r-project.org/). Normality of continuous variables distribution was assessed with a Shapiro-Wilk normality test. When variables met normality distribution, a Welch's *t*-test (variant of Student's *t*-test for samples with unequal size and variance) was adopted to run group comparisons. In cases of non-normality, Wilcoxon rank sum test was adopted as a non-parametric alternative. For subgroup-level statistics, ANalysis Of VAriance (ANOVA) was preferred in case of normality whereas Kruskal-Wallis test was used as a non-parametric alternative when needed. A Fisher's exact test was adopted when evaluating associations among discrete variables and groups. p-Values are shown for each analysis. ROI level partial correlation analyses were run with R software and the *ppcor* package (Kim, 2015), using a Spearman coefficient.

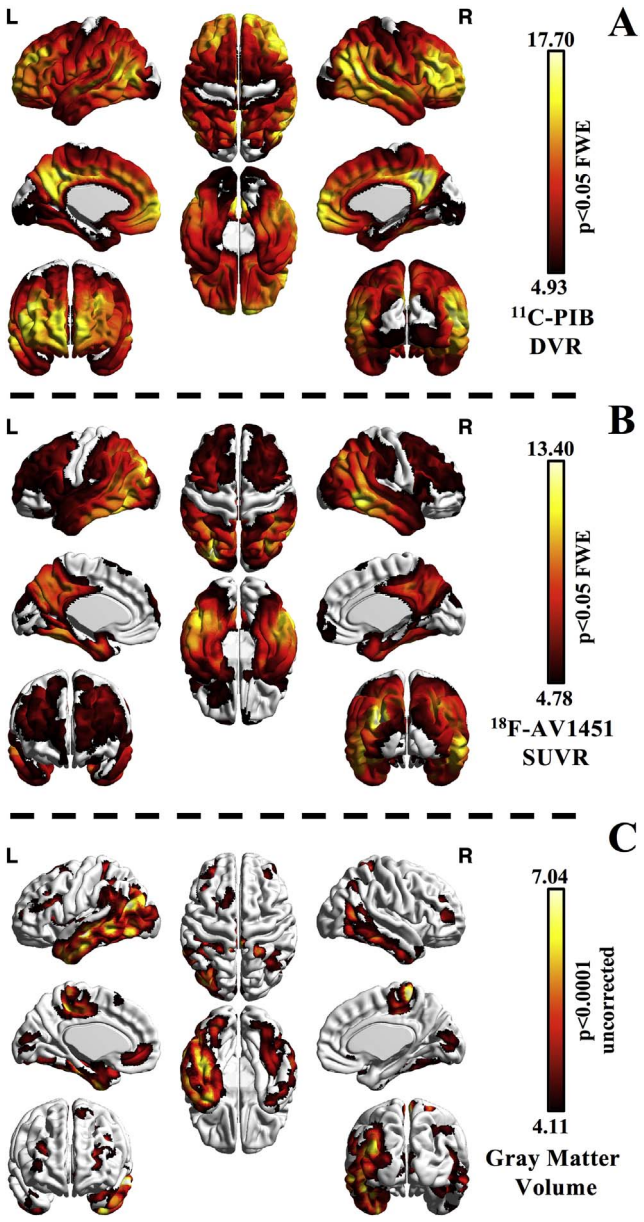

Fig. 1. Group-level pathology accumulation and neurodegeneration.
Figure showing significant amyloid accumulation (panel A, $p < 0.05$ FWE-corrected), tau accumulation (panel B, $p < 0.05$ FWE-corrected) and Gray matter volume reduction (panel C, $p < 0.0001$ uncorrected). Thresholded SPM-t maps are surface rendered on an ICBM152 template with BrainNet Viewer (see Visualization section).

2.9. Visualization

All figures were created with BrainNet software (version 1.43 [Xia et al., 2013]). In Fig. 1 the thresholded SPM-t maps were overlaid on an ICBM152 surface template provided within the software. The ranges of the color scale were relative to minimum and maximum of each SPM-t map. In Figs. 2–3 the SPM-t maps for each model were first statistically thresholded as described and then binarized. Binarized thresholded SPM-t maps were combined in a single image and then overlaid on the same surface template. In Fig. 4, Panels A–C represent inter-regional correlation visualization created with BrainNet. Each node represents a

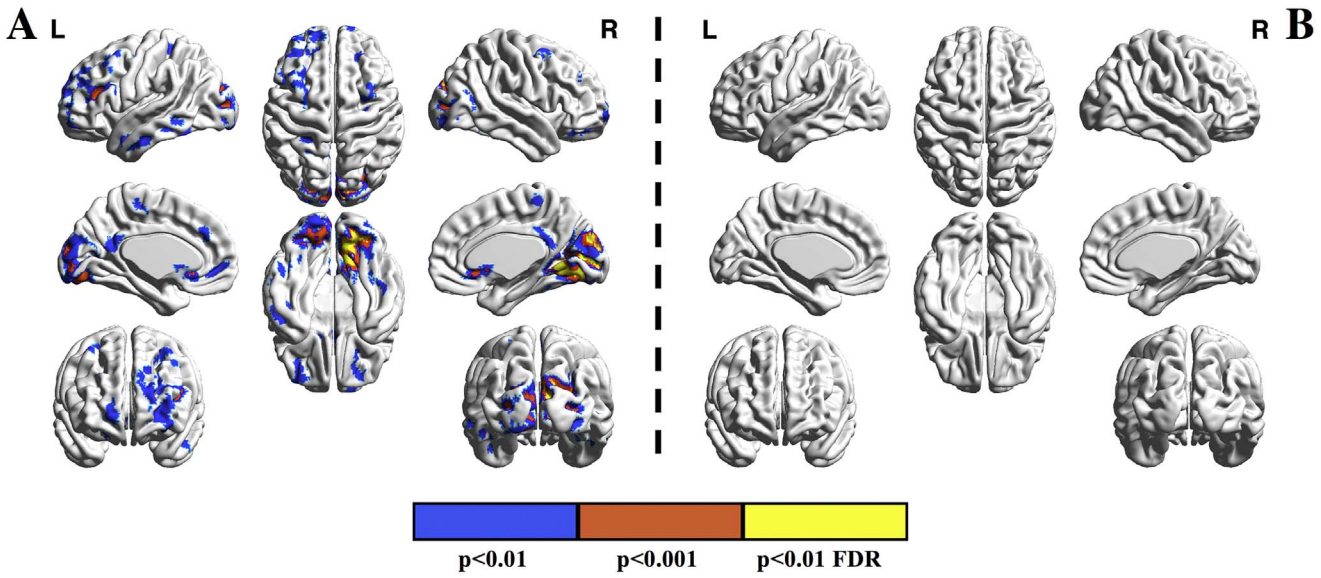

Fig. 2. BPM analysis of protein-neurodegeneration relationships.
Figure showing the results of the local multimodal Protein-Neurodegeneration BPM analysis at the voxel-level. Colors index three different statistical thresholds ranging from more liberal ($p < 0.01$ and $p < 0.001$ uncorrected for multiple comparisons) to a more conservative threshold ($p < 0.01$ FDR corrected for multiple comparisons). Thresholded SPM-t maps were binarized and summed, then surface rendered on an ICBM152 template with BrainNet Viewer (see Visualization section). Panel A: ^{18}F-AV1451 SUVR z-maps explaining GMV z-maps, controlling for age, sex and ^{11}C-PiB DVR z-maps as imaging covariate. Panel B: ^{11}C-PiB DVR z-maps explaining GMV z-maps, controlling for age, sex and ^{18}F-AV1451 SUVR z-maps as imaging covariate.

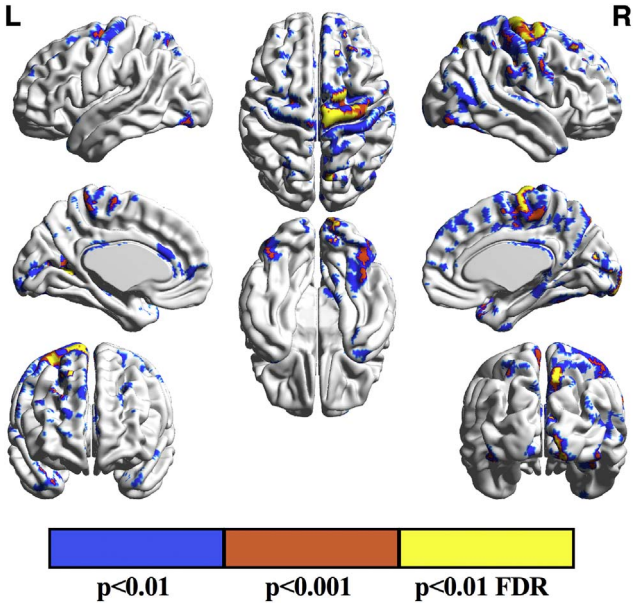

Fig. 3. BPM analysis of amyloid-tau local relationships.
Figure showing the results of the local amyloid-tau relationships BPM analysis. This model used the ^{11}C-PiB DVR z-maps as explanatory variable and ^{18}F-AV1451 SUVR z-maps as dependent variable, both PVC-corrected, controlling for age and sex. Colors index three different statistical thresholds ranging from more liberal ($p < 0.01$ and $p < 0.001$ uncorrected for multiple comparisons) to a more conservative threshold ($p < 0.01$ FDR corrected for multiple comparisons). Thresholded SPM-t maps were binarized and summed, then surface rendered on a ICBM152 template with BrainNet Viewer (see Visualization section).

cortical region segmented within the Desikan Atlas (Desikan et al., 2006) by Freesurfer software. MNI coordinates were derived from centers-of-mass of the different regions within the Desikan Atlas in standard MNI space. When needed and only for the purpose of better visualization, the coordinates were slightly changed to minimize overlap among different regions and maximize clarity. In this figure, edges are directed (and are thus represented by arrows). The direction of the arrows represents a hypothetical causal direction, *i.e.* identifying respective dependent and explanatory variables, mirroring the structures of the voxel-based regression modeling at the ROI-level. Directionality is indicated based on *a priori* hypotheses and existing literature, but is shown only for visualization purposes, since all estimates were run with a partial correlation approach which does not assume directionality.

In Fig. 4 Panel D, the stacked barplot was created with RStudio software and *ggplot2* package (Wickham, 2009). In Fig. 5 the upper panel represents correlation matrices created with RStudio software and the *ggplot2* package (Wickham, 2009). Brain inter-regional correlation visualizations were created with the same settings and software described for Fig. 4, except that the edges were not directed and were rendered with a single color.

3. Results

3.1. Demographics

The AD cohort was overall relatively young, composed of diverse phenotypes (as described above), and mildly impaired (mean MMSE 21.27 ± 6.18, CDR 0.73 ± 0.39, CDR SB 4.28 ± 2.03, Table 1). AD subgroups did not differ in terms of disease severity (Kruskal-Wallis test MMSE, $Chi^2 = 0.64$, $p = 0.726$, Clinical Dementia Rating sum of boxes $Chi^2 = 3.40$, $p = 0.183$). Patients were younger and as expected showed lower performance on the MMSE compared to HC ($p = 3.15e-06$ and $p = 7.60e-06$, respectively). Apolipoprotein E (APOE) genotype was available for 24/30 patients and for all HCs, with 11 patients (46%) and 2 HCs (17%) carrying at least one APOE e4 allele. Given the presence of missing values, APOE was not included as covariate in the multimodal correlation analyses. Global ^{11}C-PiB DVR was significantly higher in patients than HC (Welch's *t*-test, *t*-value = 19.76, $p < 2.20e-16$). There were no significant differences across patients and HCs in the delay between PET and MRI scans (Table 1).

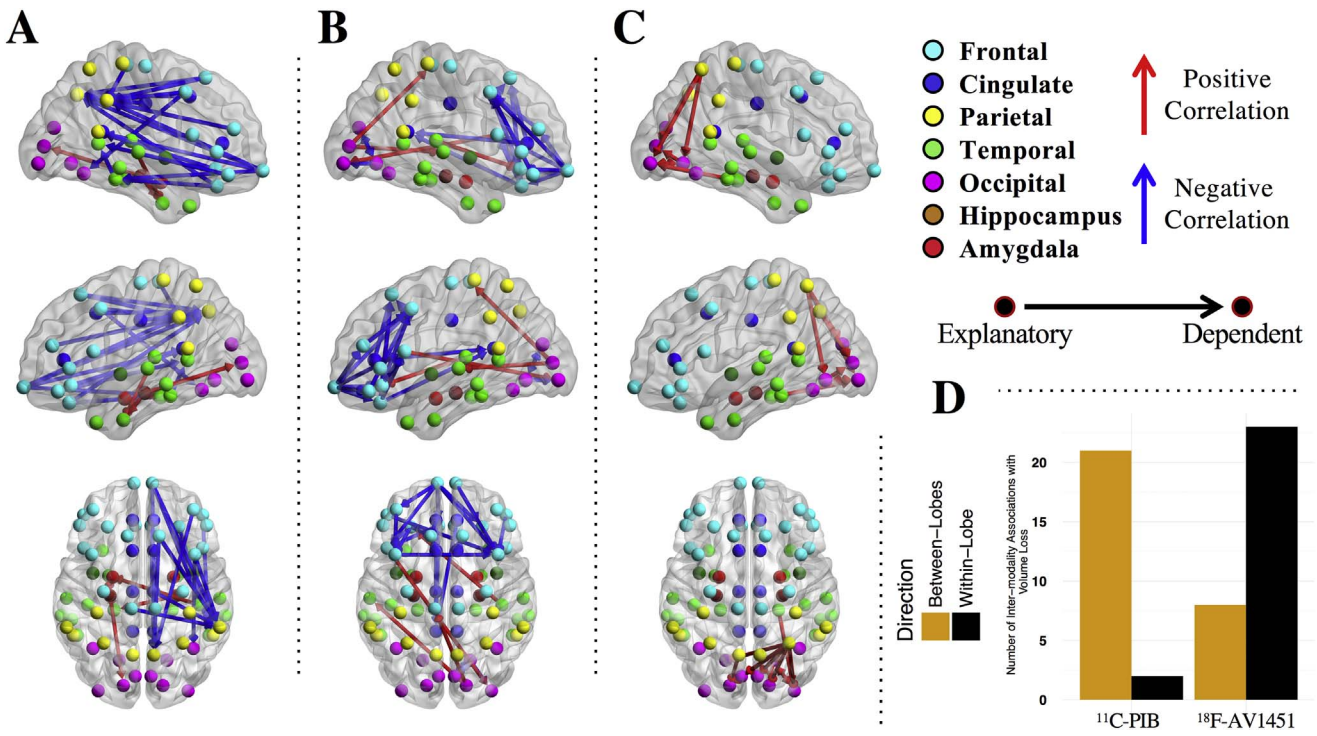

Fig. 4. Multimodal relationships between biomarkers at the ROI level.

Figure showing multimodal inter-regional relationships between ^{11}C-PiB DVR, ^{18}F-AV1451 SUVR and GMV z-scores estimated in native space. Correlation matrices are rendered on a ICBM152 template and are shown in bilateral and top axial view with BrainNet Viewer (see Visualization section). Panels A–C: Each node represents a Freesurfer-derived brain region (Desikan Atlas, see Methods). Nodes color index Macroregions. Edges color index the sign of the correlation, where BLUE = negative and RED = positive. Each edge represents a significant ($p < 0.001$ uncorrected for multiple comparisons) inter-regional correlation. (A) ^{11}C-PiB DVR z-scores explaining GMV z-scores; (B) ^{18}F-AV1451 SUVR z-scores explaining GMV z-scores; (C) ^{11}C-PiB DVR z-scores explaining ^{18}F-AV1451 SUVR z-scores (Both PVC-corrected). Panel D: Stacked barplots showing the frequency of "Within-Lobe" (black) and "Between-Lobes" (orange) associations of both ^{11}C-PiB DVR z-scores and ^{18}F-AV1451 SUVR z-scores with GMV z-scores. (For interpretation of the references to color in this figure legend, the reader is referred to the web version of this article.)

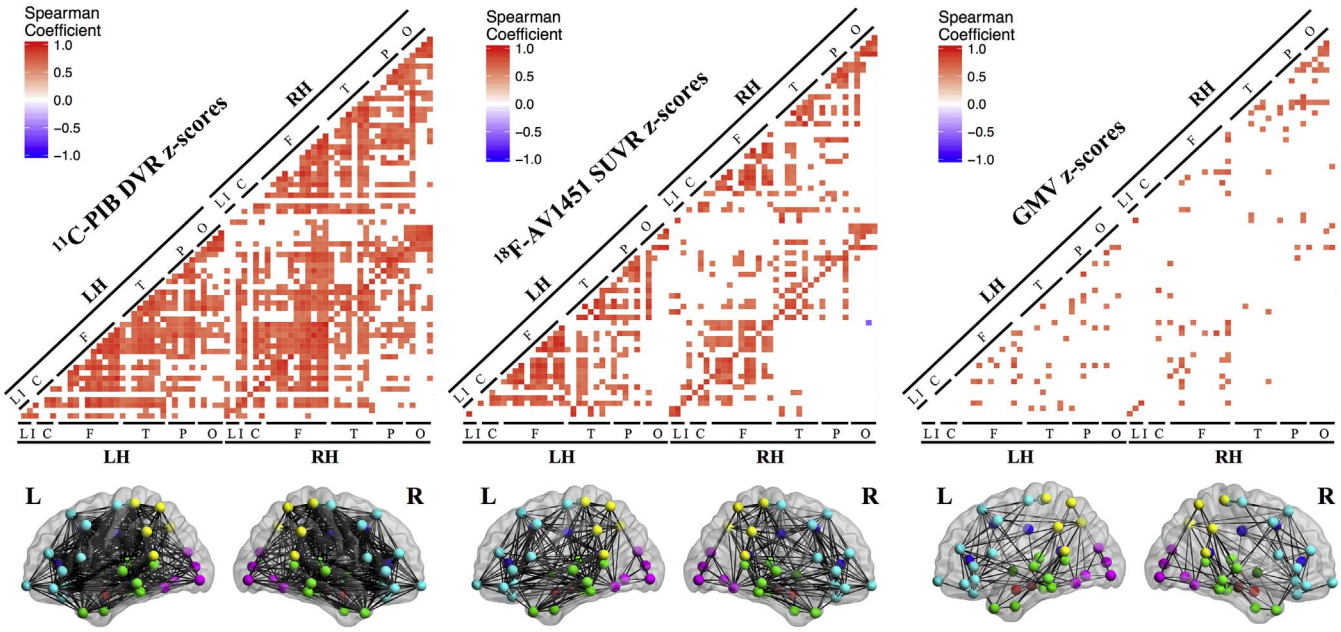

Fig. 5. Intra-modality regional correlations.

Figure showing results of intra-modal regional correlation analyses. TOP: Triangle matrices depict the intra-modal regional correlations for each biomarker studied. Color scale index partial correlation Spearman coefficient strength. Matrices are filtered to show only significant ($p < 0.001$) associations. The diagonal visible in the right lower part of all the triangles represents associations between each region and the respective contra-lateral homologue. BOTTOM: Binarized thresholded matrices are respectively rendered on a 3D surface for visualization purposes with BrainNet Viewer (see Visualization section). Each edge represents a significant inter-regional correlation (i.e. a square in the respective matrix). Within the ^{18}F-AV1451 SUVR z-scores matrix there was a single negative inter-hemispheric correlation, which was not color-coded for the purpose of visualization.

Legend: LH = left hemisphere, RH = right hemisphere, L = limbic, I = insula, C = cingulate, F = frontal, T = temporal, P = parietal, O = occipital.

Table 1
Demographic summary.

	HC	Patients	p-Value
N	12	30	–
Age (yrs)	77.25(6.82)	62.37(8.28)	**3.15e−06**
Education (yrs)	16.08(2.07)	17.17(2.96)	0.4258#
Sex (n female)	8	18	0.7402
APOE e4 carrier	2 (12 avail.)	11 (24 Avail.)	0.1427
MMSE	28.83(0.94)	21.27(6.18)	**7.60e−06#**
CDR	–	0.73(0.39)	–
CDR sb	–	4.28(2.03)	–
Global ^{11}C-PiB DVR	1.04(0.03)	1.74(0.19)	**2.20e–16**
Delay ^{18}F-AV1451-MRI (d)	58.33(39.9)	79.4(82.9)	0.9667#
Delay ^{11}C-PiB-MRI (d)	93.33(89.53)	75.97(78.27)	0.3877#
Delay ^{18}F-AV1451-^{11}C-PiB (d)	115.5(143.47)	39.03(72.41)	0.1214#

Table showing summary of demographic variables. Values are shown as mean(std) for continuous variables or counts for discrete variables. p-Values refer to either Welch's *t*-test or to a Wilcoxon rank sum test in cases of non-normality (marked with #) of the value distribution for at least one of the two groups. Legend: HC = elderly healthy controls, MMSE = mini mental state examination, APOE = Apolipoprotein E, CDR = Clinical Dementia Rating, CDR sb = Clinical Dementia Rating sum of boxes. Bold scores are significant ($p < 0.05$).

3.2. Gray matter volume reduction and protein accumulation at the voxel-level

Compared to HC, AD patients showed extensive tau and Aβ tracer retention ($p < 0.05$ FWE-corrected, Fig. 1A–B), with more spatially restricted reduction in GMV ($p < 0.0001$ uncorrected, Fig. 1C). Bilateral temporal and inferior parietal areas, predominantly on the left, showed the most consistent overlap across modalities (Fig. 1). Aβ was diffusely elevated across associative cortical regions, relatively sparing primary sensorimotor areas and peaking in medial parietal and lateral frontal regions (Fig. 1A). Tau elevation was less diffuse, targeting mostly lateral temporal, inferior parietal, lateral occipital and lateral frontal regions (Fig. 1B), relatively sparing sensorimotor areas as well. Neurodegeneration was limited (at $p < 0.0001$ uncorrected) to bilateral temporal and inferior parietal regions (L > R), slightly involving prefrontal cortices (Fig. 1C). At the more conservative $p < 0.05$ FWE-corrected threshold, GMR was evident in inferior and middle temporal lateral areas, as well as in temporo-occipital, middle cingulate and precuneus regions, with a marked left hemisphere dominance (see Supplementary file 2).

Aβ and tau accumulation peaked in different regions but their distribution largely overlapped across the evaluated brain regions. Tau accumulation and GMR peaked in the same region, *i.e.* inferior parietal lobule (Fig. 1B–C). However, GMR was more spatially restricted when compared to tau distribution, with this effect being particularly evident when applying the more conservative threshold to visualize GMR (see Supplementary file 2).

A significant local effect of tau accumulation on brain volume was revealed by the BPM analysis when taking age, sex and ^{11}C-PiB DVR z-maps into account. The effects were evident in medial, lateral and inferior occipital regions ($p < 0.01$ FDR-corrected) peaking in the right calcarine cortex (MNI coordinates 10,-90,6) and right lingual gyrus (MNI coordinates 6,-56,4). When adopting more liberal thresholds ($p < 0.001$ and $p < 0.01$ uncorrected), the effect was evident also in posterior cingulate (R > L), bilateral superior, middle and inferior occipital (R > L), left inferior temporal (L > R) and left dorsolateral prefrontal areas (L > R) (Fig. 2, Table 2). This effect was essentially unchanged when either using ^{11}C-PiB DVR global cortical values as covariates or when not adding any Aβ information into the model (data not shown).

No significant local effects of Aβ accumulation on GMR were revealed by the BPM analysis when taking age, sex and ^{18}F-AV1451 SUVR z-maps into account. The results were not altered even at liberal statistical thresholds ($p < 0.01$ uncorrected) or when taking out the ^{18}F-AV1451 SUVR z-maps as an imaging covariate (data not shown). Neither tau nor Aβ showed significant (at $p < 0.001$ uncorrected) positive associations with GMV at the voxel-level.

A significant local effect of Aβ on tau accumulation, taking age and sex into account, was observed in right frontal, parietal and medial occipital regions (more extensively in precentral gyrus, paracentral lobule and cuneus), reaching lateral middle frontal and superior parietal regions ($p < 0.01$ FDR-corrected). This effect extended to basal

Table 2
Multimodal BPM analysis.

	Label	k	SPM-t	x	y	z	p-value
A. GMV-^{18}F-AV1451 SUVR	Calcarine_R	2748	7.95	12	−86	8	1.198772e-19
	Occipital_Mid_L	208	6.49	−24	−86	16	0.0036
	Fusiform_L	588	6.04	−30	−66	−12	9.4306e-07
	Olfactory_R	123	4.78	4	12	−4	0.0409
	Frontal_Inf_Tri_L	176	4.17	−42	32	20	0.0086
B. ^{18}F-AV1451 SUVR-^{11}C-PIB DVR	Post_Cingulate_L	315	14.54	−28	−58	8	8.6398e-05
	Hippocampus_R	116	13.87	24	−40	6	0.0312
	Frontal_Mid_R	585	10.58	28	40	44	1.7464e-07
	Paracentral_Lobule_R	1323	9.18	6	−20	78	3.0309e-13
	Parietal_Sup_R	413	8.73	10	−82	50	7.8112e-06
	Cuneus_R	476	8.48	14	−90	−20	1.8431e-06
	Postcentral_R	153	8.30	46	−40	60	0.009
	Temporal_Sup_R	141	8.17	70	−22	14	0.013
	Precentral_R	111	6.90	60	12	36	0.037
	Parietal_Sup_L	221	6.57	−14	−78	58	0.001
	Temporal_Pole_Sup_R	144	6.54	30	20	−32	0.012
	Postcentral_R	167	6.30	28	−36	48	0.006
	Postcentral_R	107	5.41	62	−16	34	0.043
	Fusiform_R	213	5.41	42	−62	−22	0.001
	Occipital_Mid_L	134	5.04	−48	−86	−10	0.017
	Frontal_Sup_L	106	4.78	−26	−6	66	0.045

Table showing BPM analysis results for GMV vs. ^{18}F-AV1451 SUVR and ^{18}F-AV1451 SUVR vs. ^{11}C-PiB DVR (PVC) multiple regression models. SPM statistical threshold was set to $p < 0.001$ uncorrected for multiple comparisons, minimum cluster extent k = 100 voxels. The p-values shown are cluster-level corrected. MNI coordinates and SPM-t values of the peaks and relative anatomical labels are provided.

(A) Model with GMV z-maps as dependent variable and ^{18}F-AV1451 SUVR z-maps as explanatory variable, with age, sex and ^{11}C-PiB DVR z-maps as imaging covariates.

(B) Model with ^{18}F-AV1451 SUVR z-maps as dependent variable and ^{11}C-PiB DVR z-maps as explanatory variable, both PVC-corrected, with age and sex as non-imaging covariates.

Table 3
Protein aggregation and neurodegeneration in metaROIs.

	HC	Patients	p-Value
^{11}C-PiB DVR			
N	12	30	–
ACC	0.99(0.04)	1.56(0.18)	**9.486e–18**
PCC	1.15(0.03)	1.80(0.17)	**2.527e–20**
IFG	1.01(0.03)	1.72(0.21)	**9.891e–19**
MFG	1.03(0.04)	1.85(0.23)	**1.597e–19**
OFC	1.04(0.04)	1.76(0.24)	**3.661e–17**
SFG	1.02(0.04)	1.74(0.21)	**6.310e–19**
LOC	1.03(0.03)	1.49(0.17)	**9.869e–16**
medOC	1.05(0.03)	1.4(0.17)	**3.584e–12**
IPL	1.05(0.02)	1.70(0.18)	**1.809e−10 #**
SPL	1.07(0.05)	1.63(0.17)	**1.360e–18**
Prec	1.11(0.03)	1.96(0.2)	**1.555e–21**
LTC	0.99(0.02)	1.59(0.18)	**5.759e–18**
medTL	0.98(0.03)	1.15(0.08)	**1.251e–12**
^{18}F-AV1451 SUVR			
ACC	1.08(0.05)	1.39(0.24)	**1.175e–07**
PCC	1.10(0.08)	2.02(0.45)	**1.809e−10 #**
IFG	1.06(0.06)	1.76(0.47)	**2.17e−09 #**
MFG	0.99(0.08)	1.95(0.58)	**4.862e–10**
OFC	1.15(0.07)	1.51(0.32)	**9.68e–07**
SFG	0.98(0.09)	1.60(0.42)	**7.953e–09**
LOC	1.11(0.05)	2.02(0.42)	**5.174e–13**
medOC	1.04(0.04)	1.67(0.47)	**1.809e−10 #**
IPL	1.09(0.07)	2.45(0.56)	**3.732e−14**
SPL	1.03(0.09)	2.22(0.55)	**6.81e−13**
Prec	1.10(0.08)	2.34(0.52)	**3.163e−14**
LTC	1.10(0.05)	2.12(0.46)	**4.03e−13**
medTL	1.20(0.08)	1.47(0.23)	**1.516e−06**
Gray matter volume			
ACC	0.005(7e−04)	0.005(8e−04)	0.6741
PCC	0.006(7e−04)	0.006(8e−04)	0.7952
IFG	0.012(6e−04)	0.011(0.0013)	0.3461
MFG	0.026(0.0019)	0.023(0.0034)	**0.0023**
OFC	0.014(0.0012)	0.014(0.0018)	0.4465
SFG	0.026(0.0018)	0.026(0.0033)	0.2365
LOC	0.025(0.0015)	0.022(0.0035)	**0.0017**
medOC	0.011(0.0016)	0.011(0.002)	0.5544 #
IPL	0.027(0.0022)	0.023(0.0031)	**1.826e−05**
SPL	0.015(0.0015)	0.013(0.0022)	**0.01454 #**
Prec	0.011(9e−04)	0.01(0.0012)	**0.0089**
LTC	0.038(0.0031)	0.034(0.0049)	**0.0062**
medTL	0.009(0.0012)	0.009(0.0015)	0.6274

Table showing distribution group averages of neuroimaging measures in 13 metaROIs. Values are shown as mean(std). p-Values refer to either Welch's *t*-test or to a Wilcoxon rank sum test in case of non-normality (marked with #) of the value distribution for at least one of the two groups. Legend: HC = healthy controls, ACC = anterior cingulate cortex, PCC = posterior cingulate cortex, IFG = inferior frontal gyrus, MFG = middle frontal gyrus, OFC = orbitofrontal cortex, SFG = superior frontal gyrus, LOC = lateral occipital cortex, medOC = medial occipital cortex, IPL = inferior parietal lobule, SPL = superior parietal lobule, Prec = precuneus, LTC = lateral temporal cortex, medTL = medial temporal lobe. Bold scores are significant ($p < 0.05$).

occipital and medial frontal regions at more liberal statistical thresholds ($p < 0.001$ and $p < 0.01$ uncorrected for multiple comparisons) (see Fig. 3, Table 2). There were no significant ($p < 0.001$ uncorrected) negative associations between tau and Aβ at the voxel-level.

3.3. Gray matter volume reduction and protein accumulation at the ROI-level

Thirteen bilateral ROIs were generated by averaging the contralateral homotopic metaROIs (see Methods) and were considered for an overall summary of protein accumulation and GMV at the ROI-level. Aβ accumulation was the most prominently altered biomarker, being significantly elevated in all the evaluated regions. The peak of average ^{11}C-PiB DVR was in the precuneus (mean ± sd DVR 1.96 ± 0.20), followed by middle frontal gyrus (DVR 1.85 ± 0.23) and posterior cingulate (DVR 1.80 ± 0.17). Medial temporal lobe showed the lowest Aβ burden (DVR 1.15 ± 0.08) (Table 3). Tau accumulation was also markedly elevated across cortex, though at a lower significance than Aβ. The peak average ^{18}F-AV1451 SUVR was in the inferior parietal lobule (mean ± sd SUVR 2.45 ± 0.56), followed by precuneus (SUVR 2.34 ± 0.52) and superior parietal lobule (SUVR 2.22 ± 0.55). Of the examined cortical ROIs, anterior cingulate cortex had the lowest tau burden (SUVR 1.39 ± 0.24) (Table 3).

Gray Matter Volumes showed the most restricted differences between patients and controls, being significant ($p < 0.001$ uncorrected) only in the inferior parietal lobule (mean ± sd GMV 0.023 ± 0.0031), bilaterally with a marked prominence in the left hemisphere. In addition, middle frontal gyrus, precuneus, lateral temporal and lateral occipital cortex showed significant GMR at more liberal statistical thresholds ($p < 0.01$) (Table 3). Overall, peak tau accumulation co-localized with peak GMR in the inferior parietal lobule, while amyloid peaks were found in midline structures (*e.g.* precuneus and posterior cingulate) and lateral and medial prefrontal cortices, key hubs of the default mode network (Buckner et al., 2005).

The ROI-based partial correlation approach showed results consistent with the voxel-based BPM analyses and provided additional information on long-distance relationships between protein accumulation and GMR. The only significant ($p < 0.001$) local (intraregional) effects were found for tau accumulation on GMV in the right lingual gyrus (partial $r = -0.66$, $p = 0.0002$). A resampling analysis was performed to test the dependence of this effect on either the specific composition of our sample or on outliers. Particularly given the heterogeneous AD phenotypes included in our sample, and the known relationships between clinical presentation and regional patterns of GMR and ^{18}F-AV1451 in AD (Ossenkoppele et al., 2015a; Ridgway et al., 2012; Ossenkoppele et al., 2016; Dronse et al., 2017; Xia et al., 2017), we wanted to ensure that results were not driven by any specific sub-group of AD patients. To this purpose, a partial correlation coefficient and the relative p-value were estimated for all the possible combinations of N = 26/30 patients (*i.e. leave-four-out* approach), resulting in 27,405 iterations. All the iterations (100%) resulted in a negative Spearman coefficient (mean ± sd partial $r = -0.65 \pm 0.05$, range -0.44 to -0.84), supporting the overall negative effect of tau burden on GMV in this region in our cohort. All p-values were less than $p < 0.05$, with the majority being less than $p < 0.001$ (63% or 17,300 of the iterations). Furthermore, we continued to see a statistical trend (rho = -0.426, $p = 0.0776$) after removing all patients with PCA (which is associated with greater occipital GMR and ^{18}F-AV1451 binding compared to other AD variants), despite the significant loss of power associated with reducing our sample size.

It must be noted, however, that given the number of pairwise correlations tests included in the ROI-based analyses (N = 5184), the local effect of tau accumulation on GMR in the right lingual gyrus did not survive Bonferroni multiple comparisons correction. Therefore, the same correlation models were estimated using the bilateral metaROIs in order to reduce the number of correlations estimated (N = 169, see Supplementary file 3). At the metaROI level, inter-modal local correlations confirmed the significant negative correlation between ^{18}F-AV1451 retention and GMR in the medial occipital lobe ($r = -0.65$, $p < 0.001$), which survived Bonferroni correction for multiple comparisons ($p = 0.04$) (see Supplementary file 3).

Regional tau was negatively associated with GMV mainly in adjacent or neighboring regions (*i.e.* Within-Lobe), whereas regional Aβ was mostly associated with more distant GMR (*i.e.* Between-Lobes) (Fig. 4, Table 4). The higher proportion of Within-Lobe correlations with GMV z-scores for ^{18}F-AV1451 SUVR z-scores and Between-Lobes correlations for ^{11}C-PiB DVR z-scores was confirmed by a Fisher's exact test ($p = 1.41e-06$). The majority of negative tau effects on adjacent regional volumes were observed within the frontal and occipital lobes (Fig. 4, Table 4). Aβ burden was mostly associated with GMV in distant regions, with a prominent association between Aβ uptake in several

Table 4
Multimodal correlations in ROIs.

Direction	N	Mean r	Min r	Max r
A. ^{18}F-AV1451 - GMV				
All	31	− 0.47	− 0.69	0.68
Frontal-frontal	17	− 0.62	− 0.69	− 0.60
Occipital-occipital	4	− 0.64	− 0.67	− 0.60
Cingulate-frontal	3	− 0.63	− 0.66	− 0.60
Cingulate-cingulate	2	− 0.65	− 0.69	− 0.61
Frontal-cingulate	1	− 0.67	–	–
Frontal-occipital	1	0.61	–	–
Occipital-frontal	1	0.60	–	–
Occipital-temporal	1	0.60	–	–
Temporal-frontal	1	0.68	–	–
B. ^{11}C-PiB - GMV				
All	23	− 0.34	− 0.67	0.67
Frontal-parietal	10	− 0.61	− 0.67	− 0.59
Cingulate-parietal	3	− 0.63	− 0.67	− 0.60
Frontal-temporal	3	− 0.61	− 0.63	− 0.60
Hippocampus-temporal	3	0.65	0.63	0.67
Temporal-temporal	2	0.01	− 0.60	0.62
Frontal-occipital	1	− 0.64	–	–
Hippocampus-occipital	1	0.61	–	–
C. ^{11}C-PiB - ^{18}F-AV1451				
All	13	0.62	0.59	0.69
Parietal-occipital	8	0.62	0.60	0.65
Occipital-occipital	4	0.63	0.60	0.69
Temporal-occipital	1	0.59	–	–

Table showing summary of regional multimodal relationships resulting from partial correlation analyses. Number and mean, minimum and maximum partial r coefficients (pR) are shown for each inter-regional correlation. All regional associations were significant at $p < 0.001$ (see text). In the "Direction" column, (A–B) the first lobe represents area of protein aggregation, the second lobe represents area of GMV changes; (C) the first lobe represents area of amyloid accumulation and the second lobe represents area of tau accumulation. (A) Model with GMV z-scores as dependent variable and ^{18}F-AV1451 SUVR z-scores as explanatory variable, with age, sex and global ^{11}C-PiB DVR burden as covariates. (B) Model with GMV z-scores as dependent variable and ^{11}C-PiB DVR z-scores as explanatory variable, with age and sex as covariates. (C) Model with ^{18}F-AV1451 SUVR z-scores as dependent variable and ^{11}C-PiB DVR z-scores as explanatory variable, both PVC-corrected, with age and sex as covariates.

frontal regions and regional gray matter volumes in parietal, temporal and occipital regions. At a statistical threshold of $p < 0.001$ uncorrected, this effect was predominantly expressed in the right hemisphere (Fig. 4, Table 4). A minority of inter-regional significant correlations occurred in the opposite direction, *i.e.* elevated tracer uptake in a region being associated with increasing volume in a distant region. This was found for N = 4/31 distant GMV regional associations of ^{18}F-AV1451 and for N = 5/23 for ^{11}C-PiB. All these positive associations were between-lobes or inter-hemispheric, thus possibly reflecting partial volume effects (Fig. 4, Table 4). Aβ and tau accumulation showed significant inter-regional positive correlations ($p < 0.001$ uncorrected) in parieto-occipital regions. Right superior parietal, left precuneus, right lingual and lateral occipital and right parahippocampal Aβ was associated with tau accumulation in bilateral peri-calcarine, lingual gyrus, cuneus and right lateral occipital areas (Fig. 4, Table 4). However, no regression model using distant inter-modal correlations survived Bonferroni multiple comparisons correction, even at the metaROI level.

When examining intra-modality correlations, Aβ accumulation showed the most homogeneous inter-regional distribution, followed by tau accumulation and finally GMR. Out of a total of 2520 region-to-region combinations, 53% were significant ($p < 0.001$) for ^{11}C-PiB DVR z-scores (mean ± sd partial r = 0.71 ± 0.09), 28% were significant for ^{18}F-AV1451 SUVR z-scores (mean ± sd 0.72 ± 0.11) and 6% were significant for GMV z-scores (mean ± sd 0.66 ± 0.06) (Fig. 5). ^{11}C-PiB DVR z-scores and ^{18}F-AV1451 SUVR z-scores showed significant correlations between each region and the homologous contralateral region. GMVs showed a similar but more restricted pattern (Fig. 5).

4. Discussion

The mechanisms underlying the relationship between misfolded protein accumulation and neurodegeneration in AD are currently the focus of intense research (Herrup, 2015; Musiek and Holtzman, 2015). The complexity of this interplay is compounded by their interactions along at least two key conceptual axes, *time* and *space*. Regarding *time*, amyloid accumulation seems to begin decades before clinically apparent cognitive decline, whereas neurodegeneration seems to be temporally linked to clinical symptoms (Jack et al., 2013). Neocortical tau aggregation is likely occurring in between these events, interfering with local neuronal integrity and ultimately driving neurodegeneration. Regarding *space*, the relationships between amyloid, tau and neurodegeneration are likely to vary by both disease stage and brain region (La Joie et al., 2012). Amyloid accumulation appears to originate early on as a multi-focal process throughout large regions of association neocortex, perhaps due to shared vulnerability properties (discussed below). Neurodegeneration seems to follow later, emanating from few initial epicenters and followed by a predictable pattern of progression along inter-connected brain regions (Seeley et al., 2009; Zhou et al., 2012). Tau accumulation seems to act as a mediator, preceding and driving breakdown of specific neural circuits.

Several recent studies investigated the relationships between tau, Aβ and neurodegeneration *in vivo*, mostly at the preclinical or earliest clinical (mild cognitive impairment, MCI) stages of the disease, either considering global Aβ burden (Schöll et al., 2016; Johnson et al., 2016; Cho et al., 2016a; Hanseeuw et al., 2017) or evaluating voxel-level/regional relationships (Chiotis et al., 2016; Sepulcre et al., 2016; Brier et al., 2016; Bischof et al., 2016; Lockhart et al., 2017). The latter studies investigated multimodal associations in 88 HC (Sepulcre et al., 2016), 46 older HC (Lockhart et al., 2017), a mixed cohort of 36 HC and 10 mild AD (Brier et al., 2016), a mixed cohort of 11 prodromal AD and 9 AD dementia (Chiotis et al., 2016), and 10 patients with AD dementia (Bischof et al., 2016). Our study builds on and extends previous work by studying these relationships specifically in 30 mild AD dementia patients, a distinct "moment" in the time and space of disease evolution (Table 1). At the early stages of dementia, Aβ is elevated throughout the association neocortex, tau is elevated in temporoparietal cortices but also extends into lateral occipital and dorsolateral prefrontal regions, and atrophy is significant in temporoparietal regions. The tau distribution in Aβ positive HC seems to presage the known AD-related temporo-parietal neurodegeneration (Schöll et al., 2016), whereas in mild AD dementia it appears to presage the expected progression of neurodegeneration from temporoparietal into occipital and lateral prefrontal regions known to be involved in clinically advanced disease stages (Kim et al., 2005; McDonald et al., 2009). Our results are consistent with this proposed disease cascade, by showing that tau distribution overlapped with and exceeded GMR in the mild-AD sample. While it is tempting to speculate that tau spreading precedes future neurodegeneration, future longitudinal studies will be needed to fully test this inference.

Conversely, Aβ is elevated in regions relatively spared by atrophy even in late stages, such as medial prefrontal cortex (La Joie et al., 2012). The early pattern and spread of Aβ deposition is initially distinct from tau and atrophy, eventually converging in posterior cortices as tau and neurodegeneration spread into these regions.

Consistent with the hypothesis that tau aggregation is linked to neurodegeneration, we found local negative correlations between ^{18}F-AV1451 retention and GMV, peaking in occipital areas and particularly in the right lingual gyrus, a region involved relatively early in Braak staging of NFT pathology (Braak III, Braak et al., 2006). A similar finding was reported in a previous study investigating regional relationships between ^{18}F-AV1451 and ^{18}F-FDG-PET SUVR z-scores (Bischof et al., 2016). Of note and consistent with the present study, the authors found peak significant association between tau accumulation and neurodegeneration within occipital regions. Notwithstanding, they

also describe significant correlations within parietal, temporal and frontal regions, which were weaker in the present study (Bischof et al., 2016). Different sample compositions and the adoption of ^{18}F-FDG-PET are likely to account for these slight discordances.

ROI analyses revealed additional associations between regional tau and adjacent GMR, especially within frontal and occipital lobes. These findings may indicate that, in our cohort, relationships between tau and neurodegeneration may be approaching a plateau in temporoparietal regions where tau aggregation is highest and neurodegeneration is already advanced, whereas correlations are more readily detectable in frontal and occipital regions, where atrophy is likely to be more dynamic at this disease stage.

We did not find local associations between ^{11}C-PiB and GMV. These findings add to previous studies showing lack of cross-sectional regional relationships between Aβ and neurodegeneration (Rabinovici et al., 2010; Lehmann et al., 2013; Altmann et al., 2015; Ossenkoppele et al., 2016; Bischof et al., 2016; Xia et al., 2017; Hanseeuw et al., 2017), though other studies have reported some association, particularly in early disease stages (Cohen et al., 2009; Ossenkoppele et al., 2012; Lowe et al., 2014). ROI analyses highlighted several distant associations between Aβ burden and GMR. Most of the effect was driven by frontal Aβ correlating with temporoparietal GMR (Fig. 4, Table 4). Previous studies have described remote effects of Aβ on neurodegeneration (Laforce et al., 2014; Klupp et al., 2015). Aβ in frontal regions (as well as temporal and parietal areas) was associated with widespread atrophy in previous studies employing ^{11}C-PiB, ^{18}F-AV1451, and MRI data in HC (Sepulcre et al., 2016; Lockhart et al., 2017). These correlations may represent remote effects of Aβ *via* ongoing deafferentation (Bourgeat et al., 2010) or by triggering or accelerating tau aggregation in post-synaptic neurons connected by long-range white matter tracts, with tau mediating neurodegeneration. It is also possible that Aβ may have more local relationships with neurodegeneration at earlier disease stages (Chételat et al., 2010; Lowe et al., 2014), while tau effects predominate in a mild AD dementia cohort.

Tau accumulation in our cohort was locally associated with Aβ burden in frontal, parietal and occipital regions (Fig. 3). These results partly differ in topography from those reported in HC and earlier mixed clinical cohorts, which found peak correlations between Aβ (local and distal) and tau in temporoparietal regions (Brier et al., 2016; Chiotis et al., 2016; Sepulcre et al., 2016; Lockhart et al., 2017; Vemuri et al., 2017). The local Aβ-tau relationships were stronger in HC or in samples mostly composed of HC (Brier et al., 2016; Sepulcre et al., 2016; Lockhart et al., 2017; Vemuri et al., 2017) and less pronounced in MCI and AD dementia patients (Chiotis et al., 2016). By studying these relationships in a larger cohort of 30 patients with mild AD dementia, avoiding inclusion of HCs in the model, our study provides unique evidence corroborating the claim of tighter Aβ-tau associations in preclinical and prodromal clinical stages, weakening throughout disease progression. If amyloid and tau aggregation can be approximated by parallel, phase-shifted sigmoid curves (Jack et al., 2013), it stands to reason that different brain regions are captured at different time frames on these curves in a single cohort. In preclinical AD, these relationships may be strongest in temporal regions as tau spreads from medial to lateral temporal cortex (Sepulcre et al., 2016; Lockhart et al., 2017; Vemuri et al., 2017) whereas, in our mild AD dementia cohort, these curves may be more tightly linked in regions of advancing tau pathology in fronto-parieto-occipital cortices. While the spread of tau seems to be dependent on the co-occurrence of neocortical β-amyloid, the directionality and molecular mechanisms linking these two processes are incompletely understood. The presence of amyloid in the post-synaptic portion of the hippocampal circuit (*i.e.* posterior cingulate cortex) may trigger a transformation of tau aggregate templating in the medial temporal lobe from a relatively indolent, age-associated process to a truly pathogenic process heralding cortical spread and ultimately clinical AD (Sepulcre et al., 2016). Conversely, it has been suggested that Aβ plaques may develop in areas which receive projections from NFT-positive neurons, postulating a molecular association between presynaptic intracellular NFT and post-synaptic Aβ plaques (Ittner and Götz, 2011; Krstic and Knuesel, 2012; Duyckaerts et al., 2015; Musiek and Holtzman, 2015). Our cross-sectional data are consistent with either directionality of the Aβ-tau relationship.

In our study Aβ was the most regionally homogeneous biomarker, consistent with previous findings (Sepulcre et al., 2016; Cho et al., 2016a). This indicates that Aβ is likely to accumulate uniformly throughout large regions of association cortex (Villeneuve et al., 2015), especially in regions that are reciprocally functionally connected (Buckner et al., 2005). The peaks of Aβ spread have been hypothesized to share high metabolic demand or aerobic glycolysis (Buckner et al., 2005; Vlassenko et al., 2010), as well as "hubness" or a high number of functional connections with the rest of the brain (Buckner et al., 2009), perhaps leading to shared susceptibility to Aβ aggregation. Regional tau distribution correlated within adjacent/connected regions. This supports the notion that tau originates in specific vulnerable *loci*, then advances to other brain regions possibly following trans-synaptic spread along functional connections (Wang and Mandelkow, 2016). GMV reduction showed a similar but more restricted intra-modality correlation pattern compared to tau, consistent with a model in which neurodegeneration follows the spread of tau (Warren et al., 2012; Ossenkoppele et al., 2015a; Mattsson et al., 2016).

Our study has limitations. The studied AD patients were clinically heterogeneous. Clinical presentation in AD has been linked to region-specific differences in tau accumulation (Ossenkoppele et al., 2016; Dronse et al., 2017; Xia et al., 2017). Our permutation analyses, however, suggest that our findings were not driven by outliers. The HC group was relatively small and significantly older than the patients, and the single-subject z-maps computed based on the HCs were used for all the multimodal analyses. However, older age would minimize differences between AD patients and controls. Furthermore, our controls were all amyloid-negative, and the focus of our analysis does not rely on the composition of the control group. The cross-sectional design of this study relates the findings to a sample-specific disease stage. Longitudinal studies will be needed to investigate the dynamic relationships between Aβ, tau and neurodegeneration across the AD continuum. Lastly, intra- and inter-modality regional analyses were not corrected for multiple comparisons. We applied $p < 0.001$ as statistical threshold, in keeping with the voxel-based BPM approach, to identify reasonably robust and biologically plausible associations, balancing type-I and type-II errors. However, other than the negative effect of tau on GMV in medial occipital regions, our results did not survive Bonferroni correction for multiple comparisons and should thus be interpreted with caution.

In summary, our findings highlight that, in mild AD dementia, tau distribution spatially overlapped with and exceeded GMR in regions predicted to degenerate later in the disease course, whereas Aβ was regionally homogeneous and elevated across association neocortex. Tau showed a local link with GMR irrespective of Aβ burden, whereas Aβ effects were more distant and possibly tau-mediated. The two proteinopathies showed modest local and distal correlations compared with stronger correlations reported in earlier disease stages, suggesting that their interaction may weaken with disease progression. Finally, the relationship between tau spread and neurodegeneration reported in this and other studies suggests that therapeutic interventions aimed at slowing or curtailing the spread of tau could modify the rate of neurodegeneration and clinical progression (Yanamandra et al., 2013; Sperling et al., 2014; Pedersen and Sigurdsson, 2015).

Supplementary data to this article can be found online at https://doi.org/10.1016/j.nicl.2017.09.016.

Conflicts of interest

The authors declare no competing financial interests.

Acknowledgements & funding

This research was funded by the Italian Ministry of Education, University and Research (MIUR) (Ministerial Fellowship; to L.I.), National Institute of Neurological Disorders and Stroke (R01-NS050915; to ML.G-T.), National Institute on Deafness and Other Communication Disorders (K24 – DC015544; to ML.G-T.), National Institutes of Health (K23-AG048291; to Z.A.M.), (U54-NS092089, R01-AG038791 and U01-AG045390; to A.L.B.), National Institute on Aging grants (R01-AG045611; to G.D.R.), (R01-AG034570; to W.J.J.), (P50-AG023501; to B.L.M.), and (F32-AG050389; to S.N.L.); Tau Consortium (to A.L.B., G.D.R. and W.J.J); State of California Department of Health Services Alzheimer's Disease Research Centre of California grant (04-33516; to B.L.M); John Douglas French Alzheimer's Foundation (to G.D.R. and B.L.M.); Marie Curie FP7 International Outgoing Fellowship (628812; to R.O.); University of California (to A.L.B.), CBD Solutions (to A.L.B.), the Bluefield Project to Cure FTD (to A.L.B.), Alzheimer's Association (to A.L.B.). The donors of (Alzheimer's Disease Research), a program of BrightFocus Foundation (to R.O.); Avid Radiopharmaceuticals enabled use of the ^{18}F-AV1451 tracer, but did not provide direct funding and was not involved in data analysis or interpretation.

Commercial disclosures

L.I. has nothing to disclose. G.T. has nothing to disclose. N.A. has nothing to disclose. S.L.B has nothing to disclose. A.B. has nothing to disclose. A.L.B. receives research support from Avid, BMS, Biogen, C2N, Cortice, Eli Lilly, Forum, Genentech, Roche and TauRx for conducting clinical trials; personal compensation for consulting from Abbvie, Asceneuron, Ionis Pharmaceuticals, Janssen and Merck and serving on a DSMB for Neurogenetics; stock/options for serving on a scientific advisory board for Alector and Delos. ML.G-T. has nothing to disclose. M.J. has nothing to disclose. J.H.K. has nothing to disclose. A.L. has nothing to disclose. S.N.L. has nothing to disclose. B.L.M. serves as Medical Director for the John Douglas French Foundation; Scientific Director for the Tau Consortium; Director/Medical Advisory Board of the Larry L. Hillblom Foundation; and Scientific Advisory Board Member for the National Institute for Health Research Cambridge Biomedical Research Centre and its subunit, the Biomedical Research Unit in Dementia (UK). Z.A.M. has nothing to disclose. J.P.O. has nothing to disclose. R.O. has nothing to disclose. H.J.R. has nothing to disclose. D.R.S. has nothing to disclose. W.J.J. serves as a consultant to Bioclinica, Genentech, Novartis Pharmaceuticals. G.D.R. receives research support from Avid Radiopharmaceuticals, Eli Lilly, GE Healthcare and Piramal. He has received consulting fees and speaking honoraria from Eisai, Roche, Lundbeck, Putnam, Genentech and Merck.

References

Altmann, A., Ng, B., Landau, S.M., Jagust, W.J., Greicius, M.D., Alzheimer's Disease NeuroImaging Initiative, 2015. Regional brain hypometabolism is unrelated to regional amyloid plaque burden. Brain 138, 3734–3746.

Baker, S.L., Lockhart, S.N., Price, J.C., He, M., Huesman, R.H., Schonhaut, D., Faria, J., Rabinovici, G., Jagust, W.J., 2017. Reference tissue–based kinetic evaluation of 18F-AV-1451 for tau imaging. J. Nucl. Med. 58, 332–338.

Bischof, G.N., Jessen, F., Fliessbach, K., Dronse, J., Hammes, J., Neumaier, B., Onur, O., Fink, G.R., Kukolja, J., Drzezga, A., van Eimeren, T., Alzheimer's Disease NeuroImaging Initiative, 2016. Impact of tau and amyloid burden on glucose metabolism in Alzheimer's disease. Ann. Clin. Transl. Neurol. 3, 934–939. http://dx.doi.org/10.1002/acn3.339.

Bolmont, T., Clavaguera, F., Meyer-Luehmann, M., Herzig, M.C., Radde, R., Staufenbiel, M., Lewis, J., Hutton, M., Tolnay, M., Jucker, M., 2007. Induction of tau pathology by intracerebral infusion of amyloid-beta -containing brain extract and by amyloid-beta deposition in APP × tau transgenic mice. AJPA 171, 2012–2020. http://dx.doi.org/10.2353/ajpath.2007.070403.

Bourgeat, P., Chetelat, G., Villemagne, V.L., Fripp, J., Raniga, P., Pike, K., Acosta, O., Szoeke, C., Ourselin, S., Ames, D., Ellis, K.A., Martins, R.N., Masters, C.L., Rowe, C.C., Salvado, O., AIBL Research Group, 2010. Beta-amyloid burden in the temporal neocortex is related to hippocampal atrophy in elderly subjects without dementia. Neurology 74, 121–127.

Braak, H., Braak, E., 1991. Neuropathological stageing of Alzheimer-related changes. Acta Neuropathol. 82, 239–259.

Braak, H., Alafuzoff, I., Arzberger, T., Kretzschmar, H., Del Tredici, K., 2006. Staging of Alzheimer disease-associated neurofibrillary pathology using paraffin sections and immunocytochemistry. Acta Neuropathol. 112, 389–404.

Brettschneider, J., Del Tredici, K., Lee, V.M.Y., Trojanowski, J.Q., 2015. Spreading of pathology in neurodegenerative diseases: a focus on human studies. Nat. Rev. Neurosci. 16, 109–120.

Brier, M.R., Gordon, B., Friedrichsen, K., McCarthy, J., Stern, A., Christensen, J., Owen, C., Aldea, P., Su, Y., Hassenstab, J., Cairns, N.J., Holtzman, D.M., Fagan, A.M., Morris, J.C., Benzinger, T.L.S., Ances, B.M., 2016. Tau and Aβ imaging, CSF measures, and cognition in Alzheimer's disease. Sci. Transl. Med. 8, 338ra66.

Buckner, R.L., Snyder, A.Z., Shannon, B.J., LaRossa, G., Sachs, R., Fotenos, A.F., Sheline, Y.I., Klunk, W.E., Mathis, C.A., Morris, J.C., Mintun, M.A., 2005. Molecular, structural, and functional characterization of Alzheimer's disease: evidence for a relationship between default activity, amyloid, and memory. J. Neurosci. 25, 7709–7717.

Buckner, R.L., Sepulcre, J., Talukdar, T., Krienen, F.M., Liu, H., Hedden, T., Andrews-Hanna, J.R., Sperling, R.A., Johnson, K.A., 2009. Cortical hubs revealed by intrinsic functional connectivity: mapping, assessment of stability, and relation to Alzheimer's disease. J. Neurosci. 29, 1860–1873.

Casanova, R., Srikanth, R., Baer, A., Laurienti, P.J., Burdette, J.H., Hayasaka, S., Flowers, L., Wood, F., Maldjian, J.A., 2007. Biological parametric mapping: a statistical toolbox for multimodality brain image analysis. NeuroImage 34, 137–143.

Chételat, G., 2013. Alzheimer disease: Aβ-independent processes—rethinking preclinical AD. Nat. Rev. Neurol. 9, 123–124.

Chételat, G., Villemagne, V.L., Bourgeat, P., Pike, K.E., Jones, G., Ames, D., Ellis, K.A., Szoeke, C., Martins, R.N., O'Keefe, G.J., Salvado, O., Masters, C.L., Rowe, C.C., Australian Imaging Biomarkers and Lifestyle Research Group, 2010. Relationship between atrophy and beta-amyloid deposition in Alzheimer disease. Ann. Neurol. 67, 317–324.

Chiotis, K., Saint-Aubert, L., Savitcheva, I., Jelic, V., Andersen, P., Jonasson, M., Eriksson, J., Lubberink, M., Almkvist, O., Wall, A., Antoni, G., Nordberg, A., 2016. Imaging in-vivo tau pathology in Alzheimer's disease with THK5317 PET in a multimodal paradigm. Eur. J. Nucl. Med. Mol. Imaging 43, 1686–1699.

Cho, H., Choi, J.Y., Hwang, M.S., Kim, Y.J., Lee, H.M., Lee, H.S., Lee, J.H., Ryu, Y.H., Lee, M.S., Lyoo, C.H., 2016a. In vivo cortical spreading pattern of tau and amyloid in the Alzheimer disease spectrum. Ann. Neurol. 80, 247–258.

Cho, H., Choi, J.Y., Hwang, M.S., Lee, J.H., Kim, Y.J., Lee, H.M., Lyoo, C.H., Ryu, Y.H., Lee, M.S., 2016b. Tau PET in Alzheimer disease and mild cognitive impairment. Neurology 87, 375–383.

Cohen, A.D., Price, J.C., Weissfeld, L.A., James, J., Rosario, B.L., Bi, W., Nebes, R.D., Saxton, J.A., Snitz, B.E., Aizenstein, H.A., Wolk, D.A., DeKosky, S.T., Mathis, C.A., Klunk, W.E., 2009. Basal cerebral metabolism may modulate the cognitive effects of aβ in mild cognitive impairment: an example of brain reserve. J. Neurosci. 29, 14770–14778.

Desikan, R.S., Ségonne, F., Fischl, B., Quinn, B.T., Dickerson, B.C., Blacker, D., Buckner, R.L., Dale, A.M., Maguire, R.P., Hyman, B.T., Albert, M.S., Killiany, R.J., 2006. An automated labeling system for subdividing the human cerebral cortex on MRI scans into gyral based regions of interest. NeuroImage 31, 968–980.

Doody, R.S., Thomas, R.G., Farlow, M., Iwatsubo, T., Vellas, B., Joffe, S., Kieburtz, K., Raman, R., Sun, X., Aisen, P.S., Siemers, E., Liu-Seifert, H., Mohs, R., 2014. Phase 3 trials of solanezumab for mild-to-moderate Alzheimer's disease. N. Engl. J. Med. 370, 311–321.

Dronse, J., Fliessbach, K., Bischof, G.N., Reutern von, B., Faber, J., Hammes, J., Kuhnert, G., Neumaier, B., Onur, O.A., Kukolja, J., van Eimeren, T., Jessen, F., Fink, G.R., Klockgether, T., Drzezga, A., 2017. In vivo patterns of tau pathology, amyloid-β burden, and neuronal dysfunction in clinical variants of Alzheimer's disease. J. Alzheimers Dis. 55, 465–471.

Dubois, B., Feldman, H.H., Jacova, C., Hampel, H., Molinuevo, J.L., Blennow, K., DeKosky, S.T., Gauthier, S., Selkoe, D., Bateman, R., Cappa, S., Crutch, S., Engelborghs, S., Frisoni, G.B., Fox, N.C., Galasko, D., Habert, M.-O., Jicha, G.A., Nordberg, A., Pasquier, F., Rabinovici, G., Robert, P., Rowe, C., Salloway, S., Sarazin, M., Epelbaum, S., de Souza, L.C., Vellas, B., Visser, P.J., Schneider, L., Stern, Y., Scheltens, P., Cummings, J.L., 2014. Advancing research diagnostic criteria for Alzheimer's disease: the IWG-2 criteria. Lancet Neurol. 13, 614–629.

Duyckaerts, C., Braak, H., Brion, J.-P., Buée, L., Del Tredici, K., Goedert, M., Halliday, G., Neumann, M., Spillantini, M.G., Tolnay, M., Uchihara, T., 2015. PART is part of Alzheimer disease. Acta Neuropathol. 129, 749–756.

Giacobini, E., Gold, G., 2013. Alzheimer disease therapy—moving from amyloid-β to tau. Nat. Rev. Neurol. 9, 677–686.

Gorno-Tempini, M.L., et al., 2011. Classification of primary progressive aphasia and its variants. Neurology 76, 1006–1014.

Hanseeuw, B.J., Betensky, R.A., Schultz, A.P., Papp, K.V., Mormino, E.C., Sepulcre, J., Bark, J.S., Cosio, D.M., LaPoint, M., Chhatwal, J.P., Rentz, D.M., Sperling, R.A., Johnson, K., 2017. FDG metabolism associated with tau-amyloid interaction predicts memory decline. Ann. Neurol. 1–24. http://dx.doi.org/10.1002/ana.24910.

Hardy, J.A., Higgins, G.A., 1992. Alzheimer's disease: the amyloid cascade hypothesis. Science 256, 184–185.

Herrup, K., 2015. The case for rejecting the amyloid cascade hypothesis. Nat. Neurosci. 18, 794–799.

Hyman, B.T., Phelps, C.H., Beach, T.G., Bigio, E.H., Cairns, N.J., Carrillo, M.C., Dickson, D.W., Duyckaerts, C., Frosch, M.P., Masliah, E., Mirra, S.S., Nelson, P.T., Schneider, J.A., Thal, D.R., Thies, B., Trojanowski, J.Q., Vinters, H.V., Montine, T.J., 2012. National Institute on Aging-Alzheimer's Association guidelines for the

neuropathologic assessment of Alzheimer's disease. Alzheimers Dement. 8, 1–13.
Ittner, L.M., Götz, J., 2011. Amyloid-β and tau—a toxic pas de deux in Alzheimer's disease. Nat. Rev. Neurosci. 12, 65–72.
Jack Jr., C.R., Holtzman, D.M., 2013. Biomarker modeling of Alzheimer's disease. Neuron 80, 1347–1358.
Jack, C.R., Knopman, D.S., Jagust, W.J., Petersen, R.C., Weiner, M.W., Aisen, P.S., Shaw, L.M., Vemuri, P., Wiste, H.J., Weigand, S.D., Lesnick, T.G., Pankratz, V.S., Donohue, M.C., Trojanowski, J.Q., 2013. Tracking pathophysiological processes in Alzheimer's disease: an updated hypothetical model of dynamic biomarkers. Lancet Neurol. 12, 207–216.
Jagust, W., 2016. Is amyloid-β harmful to the brain? Insights from human imaging studies. Brain 139, 23–30.
Jansen, W.J., Ossenkoppele, R., Knol, D.L., Tijms, B.M., Scheltens, P., Verhey, F.R.J., Visser, P.J., Amyloid Biomarker Study Group, Aalten, P., Aarsland, D., Alcolea, D., Alexander, M., Almdahl, I.S., Arnold, S.E., Baldeiras, I., Barthel, H., van Berckel, B.N.M., Bibeau, K., Blennow, K., Brooks, D.J., van Buchem, M.A., Camus, V., Cavedo, E., Chen, K., Chételat, G., Cohen, A.D., Drzezga, A., Engelborghs, S., Fagan, A.M., Fladby, T., Fleisher, A.S., van der Flier, W.M., Ford, L., Förster, S., Fortea, J., Foskett, N., Frederiksen, K.S., Freund-Levi, Y., Frisoni, G.B., Froelich, L., Gabryelewicz, T., Gill, K.D., Gkatzima, O., Gómez-Tortosa, E., Gordon, M.F., Grimmer, T., Hampel, H., Hausner, L., Hellwig, S., Herukka, S.-K., Hildebrandt, H., Ishihara, L., Ivanoiu, A., Jagust, W.J., Johannsen, P., Kandimalla, R., Kapaki, E., Klimkowicz-Mrowiec, A., Klunk, W.E., Köhler, S., Koglin, N., Kornhuber, J., Kramberger, M.G., Van Laere, K., Landau, S.M., Lee, D.Y., de Leon, M., Lisetti, V., Lleó, A., Madsen, K., Maier, W., Marcusson, J., Mattsson, N., de Mendonça, A., Meulenbroek, O., Meyer, P.T., Mintun, M.A., Mok, V., Molinuevo, J.L., Møllergård, H.M., Morris, J.C., Mroczko, B., Van der Mussele, S., Na, D.L., Newberg, A., Nordberg, A., Nordlund, A., Novak, G.P., Paraskevas, G.P., Parnetti, L., Perera, G., Peters, O., Popp, J., Prabhakar, S., Rabinovici, G.D., Ramakers, I.H.G.B., Rami, L., Resende de Oliveira, C., Rinne, J.O., Rodrigue, K.M., Rodríguez-Rodríguez, E., Roe, C.M., Rot, U., Rowe, C.C., Rüther, E., Sabri, O., Sánchez-Juan, P., Santana, I., Sarazin, M., Schröder, J., Schütte, C., Seo, S.W., Soetewey, F., Soininen, H., Spiru, L., Struyfs, H., Teunissen, C.E., Tsolaki, M., Vandenberghe, R., Verbeek, M.M., Villemagne, V.L., Vos, S.J.B., van Waalwijk van Doorn, L.J.C., Waldemar, G., Wallin, A., Wallin, Å.K., Wiltfang, J., Wolk, D.A., Zboch, M., Zetterberg, H., 2015. Prevalence of cerebral amyloid pathology in persons without dementia: a meta-analysis. JAMA 313, 1924–1938. http://dx.doi.org/10.1001/jama.2015.4668.
Johnson, K.A., Schultz, A., Betensky, R.A., Becker, J.A., Sepulcre, J., Rentz, D., Mormino, E., Chhatwal, J., Amariglio, R., Papp, K., Marshall, G., Albers, M., Mauro, S., Pepin, L., Alverio, J., Judge, K., Philiossaint, M., Shoup, T., Yokell, D., Dickerson, B., Gómez-Isla, T., Hyman, B., Vasdev, N., Sperling, R., 2016. Tau positron emission tomographic imaging in aging and early Alzheimer disease. Ann. Neurol. 79, 110–119. http://dx.doi.org/10.1002/ana.24546.
Kim, S., 2015. ppcor: an R package for a fast calculation to semi-partial correlation coefficients. Commun Stat Appl Methods 22, 665–674.
Kim, E.J., Cho, S.S., Jeong, Y., Park, K.C., Kang, S.J., Kang, E., Kim, S.E., Lee, K.H., Na, D.L., 2005. Glucose metabolism in early onset versus late onset Alzheimer's disease: an SPM analysis of 120 patients. Brain 128, 1790–1801.
Klupp, E., Grimmer, T., Tahmasian, M., Sorg, C., Yakushev, I., Yousefi, B.H., Drzezga, A., Förster, S., 2015. Prefrontal hypometabolism in Alzheimer disease is related to longitudinal amyloid accumulation in remote brain regions. J. Nucl. Med. 56, 399–404.
Krstic, D., Knuesel, I., 2012. Deciphering the mechanism underlying late-onset Alzheimer disease. Nat. Rev. Neurol. 9, 25–34.
La Joie, R., Perrotin, A., Barré, L., Hommet, C., Mezenge, F., Ibazizene, M., Camus, V., Abbas, A., Landeau, B., Guilloteau, D., de La Sayette, V., Eustache, F., Desgranges, B., Chetelat, G., 2012. Region-specific hierarchy between atrophy, hypometabolism, and β-amyloid (Aβ) load in Alzheimer's disease dementia. J. Neurosci. 32, 16265–16273.
Laforce, R., Tosun, D., Ghosh, P., Lehmann, M., Madison, C.M., Weiner, M.W., Miller, B.L., Jagust, W.J., Rabinovici, G.D., 2014. Parallel ICA of FDG-PET and PiB-PET in three conditions with underlying Alzheimer's pathology. YNICL 4, 508–516.
Lehmann, M., Ghosh, P.M., Madison, C., Laforce, R., Corbetta-Rastelli, C., Weiner, M.W., Greicius, M.D., Seeley, W.W., Gorno-Tempini, M.L., Rosen, H.J., Miller, B.L., Jagust, W.J., Rabinovici, G.D., 2013. Diverging patterns of amyloid deposition and hypometabolism in clinical variants of probable Alzheimer's disease. Brain 136, 844–858.
Lockhart, S.N., Schöll, M., Baker, S.L., Ayakta, N., Swinnerton, K.N., Bell, R.K., Mellinger, T.J., Shah, V.D., O'Neil, J.P., Janabi, M., Jagust, W.J., 2017. Amyloid and tau PET demonstrate region-specific associations in normal older people. NeuroImage 150, 191–199. http://dx.doi.org/10.1016/j.neuroimage.2017.02.051.
Logan, J., Fowler, J.S., Volkow, N.D., Wang, G.J., Ding, Y.S., Alexoff, D.L., 1996. Distribution volume ratios without blood sampling from graphical analysis of PET data. J. Cereb. Blood Flow Metab. 16, 834–840.
Lowe, V.J., Weigand, S.D., Senjem, M.L., Vemuri, P., Jordan, L., Kantarci, K., Boeve, B., Jack, C.R., Knopman, D., Petersen, R.C., 2014. Association of hypometabolism and amyloid levels in aging, normal subjects. Neurology 82, 1959–1967.
Lowe, V.J., Curran, G., Fang, P., Liesinger, A.M., Josephs, K.A., Parisi, J.E., Kantarci, K., Boeve, B.F., Pandey, M.K., Bruinsma, T., Knopman, D.S., Jones, D.T., Petrucelli, L., Cook, C.N., Graff-Radford, N.R., Dickson, D.W., Petersen, R.C., Jack, C.R., Murray, M.E., 2016. An autoradiographic evaluation of AV-1451 tau PET in dementia. Acta Neuropathol. Commun. 4, 58.
Mattsson, N., Schott, J.M., Hardy, J., Turner, M.R., Zetterberg, H., 2016. Selective vulnerability in neurodegeneration: insights from clinical variants of Alzheimer's disease. J. Neurol. Neurosurg. Psychiatry 87, 1000–1004.
McDonald, C.R., McEvoy, L.K., Gharapetian, L., Fennema-Notestine, C., Hagler, D.J., Holland, D., Koyama, A., Brewer, J.B., Dale, A.M., Alzheimer's Disease NeuroImaging Initiative, 2009. Regional rates of neocortical atrophy from normal aging to early Alzheimer disease. Neurology 73, 457–465.
McKhann, G.M., Knopman, D.S., Chertkow, H., Hyman, B.T., Jack Jr., C.R., Kawas, C.H., Klunk, W.E., Koroshetz, W.J., Manly, J.J., Mayeux, R., Mohs, R.C., Morris, J.C., Rossor, M.N., Scheltens, P., Carrillo, M.C., Thies, B., Weintraub, S., Phelps, C.H., 2011. The diagnosis of dementia due to Alzheimer's disease: recommendations from the National Institute on Aging-Alzheimer's Association workgroups on diagnostic guidelines for Alzheimer's disease. Alzheimers Dement. 7, 263–269.
Mendez, M.F., Ghajarania, M., Perryman, K.M., 2002. Posterior cortical atrophy: clinical characteristics and differences compared to Alzheimer's disease. Dement. Geriatr. Cogn. Disord. 14, 33–40.
Montine, T.J., Phelps, C.H., Beach, T.G., Bigio, E.H., Cairns, N.J., Dickson, D.W., Duyckaerts, C., Frosch, M.P., Masliah, E., Mirra, S.S., Nelson, P.T., Schneider, J.A., Thal, D.R., Trojanowski, J.Q., Vinters, H.V., Hyman, B.T., National Institute on Aging, Alzheimer's Association, 2012. National Institute on Aging-Alzheimer's Association guidelines for the neuropathologic assessment of Alzheimer's disease: a practical approach. Acta Neuropathol. 123, 1–11.
Müller-Gärtner, H.W., Links, J.M., Prince, J.L., Bryan, R.N., McVeigh, E., Leal, J.P., Davatzikos, C., Frost, J.J., 1992. Measurement of radiotracer concentration in brain gray matter using positron emission tomography: MRI-based correction for partial volume effects. J. Cereb. Blood Flow Metab. 12, 571–583.
Murray, M.E., Lowe, V.J., Graff-Radford, N.R., Liesinger, A.M., Cannon, A., Przybelski, S.A., Rawal, B., Parisi, J.E., Petersen, R.C., Kantarci, K., Ross, O.A., Duara, R., Knopman, D.S., Jack, C.R., Dickson, D.W., 2015. Clinicopathologic and 11C-Pittsburgh compound B implications of Thal amyloid phase across the Alzheimer's disease spectrum. Brain 138, 1370–1381.
Musiek, E.S., Holtzman, D.M., 2015. Three dimensions of the amyloid hypothesis: time, space and 'wingmen'. Nat. Neurosci. 18, 800–806.
Nelson, P.T., et al., 2012. Correlation of Alzheimer disease neuropathologic changes with cognitive status: a review of the literature. J. Neuropathol. Exp. Neurol. 71, 362–381.
Okamura, N., Harada, R., Furukawa, K., Furumoto, S., Tago, T., Yanai, K., Arai, H., Kudo, Y., 2016. Advances in the development of tau PET radiotracers and their clinical applications. Ageing Res. Rev. 30, 107–113.
Ossenkoppele, R., Zwan, M.D., Tolboom, N., van Assema, D.M.E., Adriaanse, S.F., Kloet, R.W., Boellaard, R., Windhorst, A.D., Barkhof, F., Lammertsma, A.A., Scheltens, P., van der Flier, W.M., van Berckel, B.N.M., 2012. Amyloid burden and metabolic function in early-onset Alzheimer's disease: parietal lobe involvement. Brain 135, 2115–2125.
Ossenkoppele, R., Cohn-Sheehy, B.I., La Joie, R., Vogel, J.W., Möller, C., Lehmann, M., van Berckel, B.N.M., Seeley, W.W., Pijnenburg, Y.A., Gorno-Tempini, M.L., Kramer, J.H., Barkhof, F., Rosen, H.J., van der Flier, W.M., Jagust, W.J., Miller, B.L., Scheltens, P., Rabinovici, G.D., 2015a. Atrophy patterns in early clinical stages across distinct phenotypes of Alzheimer's disease. Hum. Brain Mapp. 36, 4421–4437.
Ossenkoppele, R., Schonhaut, D.R., Baker, S.L., O'Neil, J.P., Janabi, M., Ghosh, P.M., Santos, M., Miller, Z.A., Bettcher, B.M., Gorno-Tempini, M.L., Miller, B.L., Jagust, W.J., Rabinovici, G.D., 2015b. Tau, amyloid, and hypometabolism in a patient with posterior cortical atrophy. Ann. Neurol. 77, 338–342.
Ossenkoppele, R., Schonhaut, D.R., Schöll, M., Lockhart, S.N., Ayakta, N., Baker, S.L., O'Neil, J.P., Janabi, M., Lazaris, A., Cantwell, A., Vogel, J., Santos, M., Miller, Z.A., Bettcher, B.M., Vossel, K.A., Kramer, J.H., Gorno-Tempini, M.L., Miller, B.L., Jagust, W.J., Rabinovici, G.D., 2016. Tau PET patterns mirror clinical and neuroanatomical variability in Alzheimer's disease. Brain 139, 1551–1567. http://dx.doi.org/10.1093/brain/aww027.
Pedersen, J.T., Sigurdsson, E.M., 2015. Tau immunotherapy for Alzheimer's disease. Trends Mol. Med. 21, 394–402.
Pontecorvo, M.J., Devous, M.D., Navitsky, M., Lu, M., Salloway, S., Schaerf, F.W., Jennings, D., Arora, A.K., McGeehan, A., Lim, N.C., Xiong, H., Joshi, A.D., Siderowf, A., Mintun, M.A., 18F-AV-1451-A05 investigators, 2017. Relationships between flortaucipir PET tau binding and amyloid burden, clinical diagnosis, age and cognition. Brain 140, 748–763. http://dx.doi.org/10.1093/brain/aww334.
Querfurth, H.W., Laferla, F.M., 2010. Alzheimer's disease. N. Engl. J. Med. 362, 329–344.
Rabinovici, G.D., Furst, A.J., Alkalay, A., Racine, C.A., O'Neil, J.P., Janabi, M., Baker, S.L., Agarwal, N., Bonasera, S.J., Mormino, E.C., Weiner, M.W., Gorno-Tempini, M.L., Rosen, H.J., Miller, B.L., Jagust, W.J., 2010. Increased metabolic vulnerability in early-onset Alzheimer's disease is not related to amyloid burden. Brain 133, 512–528.
Ridgway, G.R., Lehmann, M., Barnes, J., Rohrer, J.D., Warren, J.D., Crutch, S.J., Fox, N.C., 2012. Early-onset Alzheimer disease clinical variants: multivariate analyses of cortical thickness. Neurology 79, 80–84. http://dx.doi.org/10.1212/WNL.0b013e31825dce28.
Salloway, S., et al., 2014. Two phase 3 trials of bapineuzumab in mild-to-moderate Alzheimer's disease. N. Engl. J. Med. 370, 322–333.
Schöll, M., Lockhart, S.N., Schonhaut, D.R., O'Neil, J.P., Janabi, M., Ossenkoppele, R., Baker, S.L., Vogel, J.W., Faria, J., Schwimmer, H.D., Rabinovici, G.D., Jagust, W.J., 2016. PET imaging of tau deposition in the aging human brain. Neuron 89, 971–982.
Seeley, W.W., Crawford, R.K., Zhou, J., Miller, B.L., Greicius, M.D., 2009. Neurodegenerative diseases target large-scale human brain networks. Neuron 62, 42–52.
Sepulcre, J., Schultz, A.P., Sabuncu, M., Gómez-Isla, T., Chhatwal, J., Becker, A., Sperling, R., Johnson, K.A., 2016. In vivo tau, amyloid, and gray matter profiles in the aging brain. J. Neurosci. 36, 7364–7374.
Sevigny, J., et al., 2016. The antibody aducanumab reduces Aβ plaques in Alzheimer's disease. Nature 537, 50–56.
Sperling, R., Mormino, E., Johnson, K., 2014. The evolution of preclinical Alzheimer's disease: implications for prevention trials. Neuron 84, 608–622.
Spires-Jones, T.L., Hyman, B.T., 2014. The intersection of amyloid beta and tau at synapses in Alzheimer's disease. Neuron 82, 756–771.
Vasconcelos, B., Stancu, I.-C., Buist, A., Bird, M., Wang, P., Vanoosthuyse, A., Van Kolen,

K., Verheyen, A., Kienlen-Campard, P., Octave, J.-N., Baatsen, P., Moechars, D., Dewachter, I., 2016. Heterotypic seeding of tau fibrillization by pre-aggregated Abeta provides potent seeds for prion-like seeding and propagation of tau-pathology in vivo. Acta Neuropathol. 131, 549–569. http://dx.doi.org/10.1007/s00401-015-1525-x.

Vemuri, P., Lowe, V.J., Knopman, D.S., Senjem, M.L., Kemp, B.J., Schwarz, C.G., Przybelski, S.A., Machulda, M.M., Petersen, R.C., Jack, C.R., 2017. Tau-PET uptake: regional variation in average SUVR and impact of amyloid deposition. Alzheimers Dement. 6, 21–30. http://dx.doi.org/10.1016/j.dadm.2016.12.010.

Villemagne, V.L., Fodero-Tavoletti, M.T., Masters, C.L., Rowe, C.C., 2015. Tau imaging: early progress and future directions. Lancet Neurol. 14, 114–124.

Villeneuve, S., et al., 2015. Existing Pittsburgh compound-B positron emission tomography thresholds are too high: statistical and pathological evaluation. Brain 138, 2020–2033.

Vlassenko, A.G., Vaishnavi, S.N., Couture, L., Sacco, D., Shannon, B.J., Mach, R.H., Morris, J.C., Raichle, M.E., Mintun, M.A., 2010. Spatial correlation between brain aerobic glycolysis and amyloid-β (Aβ) deposition. Proc. Natl. Acad. Sci. U. S. A. 107, 17763–17767.

Wang, Y., Mandelkow, E., 2016. Tau in physiology and pathology. Nat. Rev. Neurosci. 17, 5–21.

Warren, J.D., Fletcher, P.D., Golden, H.L., 2012. The paradox of syndromic diversity in Alzheimer disease. Nat. Rev. Neurol. 8, 451–464.

Wickham, H., 2009. ggplot2. Springer New York, New York, NY.

Xia, M., Wang, J., He, Y., 2013. BrainNet viewer: a network visualization tool for human brain connectomics. PLoS ONE 8, e68910.

Xia, C., Makaretz, S.J., Caso, C., McGinnis, S., Gomperts, S.N., Sepulcre, J., Gómez-Isla, T., Hyman, B.T., Schultz, A., Vasdev, N., Johnson, K.A., Dickerson, B.C., 2017. Association of in vivo [18F]AV-1451 tau PET imaging results with cortical atrophy and symptoms in typical and atypical Alzheimer disease. JAMA Neurol. http://dx.doi.org/10.1001/jamaneurol.2016.5755.

Yanamandra, K., Kfoury, N., Jiang, H., Mahan, T.E., Ma, S., Maloney, S.E., Wozniak, D.F., Diamond, M.I., Holtzman, D.M., 2013. Anti-tau antibodies that block tau aggregate seeding in vitro markedly decrease pathology and improve cognition in vivo. Neuron 80, 402–414.

Yang, X., Beason-Held, L., Resnick, S.M., Landman, B.A., 2011. Biological parametric mapping with robust and non-parametric statistics. NeuroImage 57, 423–430.

Zhou, J., Gennatas, E.D., Kramer, J.H., Miller, B.L., Seeley, W.W., 2012. Predicting regional neurodegeneration from the healthy brain functional connectome. Neuron 73, 1216–1227.